جامعة أبو بكر بلقايد
UNIVERSITÉ DE TLEMCEN

Pan African University
Institute of Water and Energy Sciences

Institute of Water and Energy Sciences (Including Climate Change)

Study of impact of climate change on surface water through hydrological modeling: case of Dano Catchment in Burkina-Faso

NGAGUE HISSEINE GANDA

Date: 0?/09/2018

Master in ***Water, Engineering track***

President:

Supervisor: Dr Yaovi Aymar BOSSA

Co-supervisor: Dr Yacouba YIRA

External Examiner:

Internal Examiner:

Academic Year: 2017-2018

DECLARATION

I, NGAGUE HISSEINE GANDA hereby declare that this thesis represents my personal work, realized to the best of my knowledge. I also declare that all information, material and results from other works presented here, have been fully cited and referenced in accordance with the academic rules and ethics.

Signed:

Name NGAGUE HISSEINE GANDA **Date :** 08 /14/ 2018

Abstract

Climate change is one of the most complex and sensitive issues at the beginning of the twenty-first century. In Burkina Faso, a Sahel country, the problem of water resources is closely linked to rainfall, which is both low and uncertain. In the last 40 years, rainfall has been steadily declining, with periods of increased drought, especially in the 1970s and 1980s. These events have altered the hydrology of the basins of the zone.

The current work applied five regional climate model products and two conceptual hydrological simulation models to assess climate change impact on water resources in the Dano catchment. The projected climate change signal for the catchment was analyzed through the comparison between two future periods (P1: 2021-2050 & P2: 2071-2100) and the historical period (1976-2005). The impact of the detected climate change signal on surface water was then assessed using hydrological models HBV-light and GR4J that were successfully validated (NSE= 0.85 and R^2=0.88 for HBV-light and GR4J NSE = 0.85 and R^2 = 0.83 respectively)

The results indicate for climate change that: (i) the temperature will increase from 0.1 to 2.8 ° C for the five regional climate products; (ii) precipitation will increase by 20.92% on P1 and 3.28% on P2 according to the ESM-CCLM model, by 1.42% on P1 according to the HadGEM2-RCA model and by 0.51% on P1 according to the ESM-REMO model while the models HadGEM2-CCLM, HadGEM2-RCA, ESM-RCA and ESM-REMO instead project respective decreases of P1 = -2.71% and P2 = -3.07%; P2 = -2.16%; P1 = -8.35% and P2 = -2.89% and P2 = 17.12%.

The projected discharge change signals are consistent with the projected precipitation change signal: (i) a decrease of -12.63 mm on P1 and -16.29 mm on P2 for the HadGEM2-CCLM model, - 11.67 mm for the HadGEM2 model -RCA, and for the ESM-RCA and ESM-REMO models a respective decrease of -1.69 mm on P1 and -34.60 mm on P2; -23.93 on P1 and -47.48 mm on P2, and an increase for the ESM-CCLM models (P1 = 63.56 mm and P2 = 3.60 mm) and HadGEM2-RCA (P1 = 6.16 mm). These trends are similar for both hydrological models, but the magnitude of the change is higher with HBV-light than with GR4J.

These results suggest for future surface water resources management under climate change in the catchment to consider both discharge increase and decrease as the study shows that both trends are plausible. Under increased discharge conditions flood and erosion risk will increase,

while water shortage due to flow cessation will be more prominent under decreasing discharge conditions. Therefore, adaptation measures to cope with climate change impact on surface water resources in the Dano catchment should be tailored considering both directions; they should include soil and water conservation technics that are valid under both projected discharge trends.

Keywords: Climate change, Hydrological modeling, Burkina Faso, HBV-light and GR4J.

Résumé

Le changement climatique est l'une des questions les plus complexes et les plus sensibles au début du XXIe siècle. Au Burkina Faso, pays du Sahel, le problème des ressources en eau est étroitement lié aux précipitations, à la fois faibles et incertaines. Au cours des 40 dernières années, les précipitations ont régulièrement diminué, avec des périodes de sécheresse accrue, en particulier dans les années 70 et 80. Ces événements ont altéré l'hydrologie des bassins de la zone.

Le présent travail a consisté en l'application de cinq modèles climatiques régionaux et deux modèles hydrologiques conceptuels pour évaluer l'impact des changements climatiques sur les ressources en eau dans le bassin versant de Dano. Le signal de changement climatique projeté pour le bassin versant a été analysé à travers la comparaison entre deux périodes futures (P1: 2021-2050 & P2: 2071-2100) et la période historique (1976-2005). L'impact du signal de changement climatique détecté sur les eaux de surface a ensuite été évalué à l'aide de modèles hydrologiques HBV-light et GR4J qui ont été validés avec succès (NSE = 0,85 et R2 = 0,88 pour HBV-light et GR4J NSE = 0,85 et R2 = 0,83 respectivement)

Les résultats indiquent pour le changement climatique que: (i) la température augmentera de 0.1 à 2.8 °C pour les cinq produits climatiques régionaux; (ii) les précipitations augmenteront de 20.92% sur P1 et 3.28% sur P2 selon le modèle ESM-CCLM, de 1.42% sur P1 selon le modèle HadGEM2-RCA et de 0.51 % sur P1 selon le modèle ESM-REMO tandis que les modèles HadGEM2-CCLM, HadGEM2-RCA, ESM-RCA et ESM-REMO projettent plutôt des diminutions respectives de P1 = -2.71% et P2 = -3.07 % ; P2 = -2.16 % ; P1 = -8.35 % et P2 = -2.89 % et P2 = 17.12 %.

Les signaux de changement de décharge projetés sont cohérents avec le signal de changement de précipitation projeté : (i) une diminution de -12.63 mm sur P1 et -16.29 mm sur P2 pour le modèle HadGEM2-CCLM, de – 11.67 mm pour le modèle HadGEM2-RCA, et pour les modèles ESM-RCA et ESM-REMO une diminution respective de -1.69 mm sur P1 et -34.60 mm sur P2 ; -23.93 sur P1 et -47.48 mm sur P2, et une augmentation pour les modèles ESM-CCLM (P1 = 63.56 mm et P2 = 3.60 mm) et HadGEM2-RCA (P1= 6.16 mm) . Ces tendances sont similaires pour les deux modèles hydrologiques, mais l'ampleur du changement est plus élevée avec HBV-light qu'avec GR4J.

Mots clés : Changement climatique, Modélisation hydrologique, Burkina Faso, HBV-light et GR4J.

Acknowledgement

This research has been a success thanks to the collective efforts of many organizations and individuals. I would like to express my deep gratitude to:

- The Pan African University of Water and Energy Sciences, including Climate Change, the director and his team and guest speakers;
- German partner GIZ for technical and financial support;
- My supervisor, Dr Yaovi Aymar BOSSA, for his attentive advice and for having accepted to welcome me to the WASCAL Competence Center for my end of study internship;
- My co-supervisor, Dr. Yacouba YIRA, for his thoughtful advice, the effort and time spent on this Thesis;
- Wascal competence center and his personal for their availability and precious help.
- To my friends and colleagues for their comments and helpful comments.

Dedication

I dedicate this work

To my father NGAGUE SAKOU HAOU and my mother Amina ABDELBANAT, who have unconditionally supported me,

To brothers and sisters.

Table of contents

LIST OF ABBREVIATIONS AND ACRONYMS

HadGEM2-CCLM	MOHC-HadGEM2-ES_CLMcom-CCLM
HadGEM2-RCA	MOHC-HadGEM2-ES_SMHI-RCA
ESM-CCLM	MPI-M-MPI-ESM-LR_CLMcom-CCLM
ESM-REMO	MPI-M-MPI-ESM-LR_MPI-REMO
ESM-RCA	MPI-M-MPI-ESM-LR_SMHI-RCA
ETP	Potential evapotranspiration
P1	Projection 2021-2050
P2	Projection 2071-2100
R^2	Coefficient of determination
Nash	Sutcliffe criterion calculated on streamflow values
DGRE	General Directorate of Water Resources
PSA	Plan stratégique pour le traitement des eaux usées et des excréments du centre-ville de Dano
WASCAL	West African Science Service Centre on Climate Change

List of tables

List of figures

CHAPTER 1
GENERAL INTRODUCTION

I. General introduction

1.1. Introduction

Climate change is one of the most complex and sensitive issues at the beginning of the twenty-first century. They are as complex as an equation with many unknowns. As mentioned, at the United Nations General Assembly on Climate Change on September 23, 2014, by Sam Kutesa (the representative of Uganda).) climate change is an urgent challenge and a potentially irreversible threat to livelihoods. Considering the context of Earth's limited natural resources and assimilation capacity, the pressure of humankind on these natural resources is not sustainable (Hoekstra and Wiedmann, 2014). Most methods used in the past have dangerously and lastingly deteriorated and destroyed the planet's resources. Thus, there are no issues that are fraught with consequences for the future of humanity as the issue of climate change. The long-term consequences, or even their irreversibility, threaten the life of today and jeopardize the future of future generations; as environmental degradation compromises the economic, social development goals of our century (Millennium ecosystem service assessment-MEA, 2005).

Assessing the impact of climate change on stream flow is essential to understanding changes in water resources and improving water resources management. Indeed, climate change can seriously disrupt regional hydrology and thus affect human societies and life in general (Teutschbein, 2013).

The prospect of climate change raises many questions about the future of water resources in West Africa. In that sense Tristan d'Orgeval, (2008) argues that one of the crucial issues for the future planning of water resources and agricultural resources is the impact of climate change on rainfall in West Africa, then the impact of this rainfall on the continental water cycle.

Indeed, water in these areas is a determining factor for many human activities such as agriculture, electricity production or drinking water supply (Bodian et al., 2013).In recent decades, Burkina Faso, a Sahel country, has faced a series of "extreme" climatic events of unprecedented scale and speed. One can think in particular of the dry periods of the last three decades of which the most affected years were 1973-74 and 1983-84 (Kasei et al., 2010) and which greatly affected the ecosystems as well as the production systems of Burkina Faso. The country's desertification has serious biophysical, socio-economic and hydrosphere consequences. Several recent studies have assessed the historical evolution of climatic parameters (rainfall, temperature, evapotranspiration) and surface water resources in Burkina Faso. For regional water management in general, and

Burkina Faso in particular, the influence of climate change on water resources and hydrological systems can be reflected in both content and approaches, such as the intensity and frequency of extreme rainfall events, quantity of water available locally and the vulnerability and management of water resources systems(Roudier et al., 2014).

1.2.Problem Statement

Inadequate freshwater is one of the major current and future challenges facing Africa (Bates et al., 2008) . According to UNEP / GRID-Arendal, (2002), water availability in twelve African countries (including Burkina Faso) is expected to be between 1000 and 1700 m3 / person / year by 2025 and water stress could reach 460 million people mainly in West Africa.

Increasing demography highlights the problem of the availability of water resources. According to ECOWAS (Economic Community of West African States) (2017) the population of the ECOWES region will be around one billion and that of Burkina Faso will reach more than 60 million by 2050. These demographic projections clearly announce that the pressure on the water in the coming years will continue while accelerating.

In addition to this demographic pressure on water, rain, the main source of fresh water, is subject to spatial and temporal variability. Numerous analyzes (Carbonnel and Hubert, 1992, Sircoulon, 1990, ülivry et al., 1993, Nicholson, 1994, Mahé and ülivry, 1995, Paturel et al., 1997, Servat et al., 1997) have shown that rainfall has been remarkably below average in parts of Africa in the 1970s and 1980s, while the previous two decades have been relatively wet.

The global average temperature has increased by 0.6 ° over the last century with the hottest years ever recorded after 1990 (Serigne Tacko Kandji et al., 2006). Models based on climate change due to greenhouse gases clearly suggest that the warming of Africa will continue to reach an average annual increase of between 2 ° and 6 ° C by 2100 (Hulme et al., 2001).

According to (Zhu et al., 2017) Climate change is expected to cause significant variation in hydrological systems and the water cycle by altering the radiative equilibrium of the atmosphere, which can lead to changes in climatic variables such as pressure, temperature, precipitation and others. For example, Abubakari et al. (2017) note that rainfall intensities, as well as rainfall amounts in West Africa show a high temporal variability increasing the vulnerability of the population to climate change. Ouedraogo (2001) also reported that in Burkina Faso, Cote d'Ivoire

and Mali zone, the annual rainfall deficit varies between 10 and 40%, whereas the average annual flows have a deficit greater than 20% and exceeding a few times 60%.

It is imperative for Burkina Faso, which is part of this Sahel region, to meet climate change challenges. For many areas in Burkina Faso, surface water resources are the main water resource. The country invested in the construction of about 1,500 water reservoirs spread throughout Burkina Faso between 1960-2018 (DGRE). The pressure is even greater on the Sudano-Sahel sub-basins of Burkina Faso; whose rainfall variability has a direct impact on these water resources.

1.3. Justification

In West Africa, surface water resources of major river basins record significant intra/interannual fluctuations due to climate change and climate variability observed in the region (Sircoulon, 1987). This is the case of the watershed of the city of Dano in Burkina Faso where well evidenced effects of climate change are reported. Indeed, (Waongo et al., 2015) observed an average temperature increase of + 0.31 ° C / decade and + 0.17 ° C / decade, respectively for the minimum and maximum temperature for the region taking into account the period 1960-2010. This phenomenon, which causes an increase of evapotranspiration, has led to a reduction in the volume of water in this basin during the last decades. This goes hand in hand with a decrease in rainfall in the city of Dano also resulting from climatic variations. This can have a direct consequence on water availability.

Very few studies on climate change impact on water resources have been carried out in the Dano watershed. To date, the only two reported cases are from Op de Hipt et al. (2018) and Yira et al. (2017). These studies reported unclear behavior of future climate change and it impact on water resources for the Dano watershed. Moreover, both studies applied each a single hydrological model; thus, did not investigated the uncertainty related to the choice of the hydrological simulation model, as proposed in the frame of the current study that applied two hydrological models. Furthermore, the current study widens the basis of climate models used in climate change impacts assessment for the Dano watershed. Hence, the study provides (i) a complementary understanding of climate change impact on water resources in the Dano catchment; and (ii) an additional uncertainty analysis element that is the choice of the hydrological model used in the hydrological impact assessment of climate change.

This justifies the interest of our study through the theme "Study of the impact of climate change on the water by the hydrological model: case of Dano Basin in Burkina Faso".

1.4. Objective

The current study provides insights for the management of water resources in the Dano watershed under changing climate conditions. Its overall objective is to evaluate the impacts of climate change on surface water in the Dano Basin in Burkina Faso by means of hydrological modeling.

The specific objectives of the study are to*:*

1. Analyze projected climate change signal of the catchment
2. Model the hydrological regime of the Dano catchment using Hbv-light and GR4J.
3. Evaluate the impacts of climate change on surface water.
4. Propose mitigation and adaptation measures.

1.5. Research Questions

This paper, which focuses on the study of the impacts of climate change on surface water resources in the Dano Catchment in Burkina Faso, seeks to provide answers to the following questions:

- What are the projected climate change signals for the Dano catchment under climate change scenario RCP4.5?
- What is the resulting projected change in surface water for the catchment by 2050 and 2100?
- How is the choice of the hydrological model affecting the projected discharge change in catchment?
- What are the strategies to minimize the impacts of climate change on water surface water resources in the catchment?

Chapter 2
LITERATURE REVIEW

II. Climate, hydrological modeling, and climate impact assessment

2.1. Climate

Climate is the long-term state of the atmosphere - a synthesis of time over a statistically significant period (30 years according to the World Meteorological Organization. For IPCC (2001) “Climate refers to the average time in terms of mean and variability over a period of time and in a certain area. Classic climatology provides a classification and description of the various weather patterns found on Earth. The climate varies from place to place other, according to latitude, distance to the sea, vegetation, presence or absence of mountains or other geographical factors. The climate also varies in time, from year to year, from year to year, decade to decade, or much longer time scales, such as ice age.

Max Sorre (2010)defines the climate as the atmospheric ambience constituted by the series of states of the atmosphere above a place in their usual succession. The climate is also different according to the regions (equatorial, tropical, temperate, etc).

2.2. Climate variation

Climate variability represents changes in mean status and other statistical climate variables at all temporal and spatial scales other than specific meteorological phenomena. (Diallo and Sanda, 2009)

In other words, it is the natural variation within and between years of the climate. It is an inherent feature of the climate that manifests itself in the differences between the long-term statistics of climatic elements (rainfall, temperature, humidity, season duration) calculated for different periods. The variability of the climate is often perceived through the irregularity of climatic parameters in their evolution. According to Schmoldt et al., (1975), Africa is particularly vulnerable to climate variability in view of its economies largely based on agropastoral production systems that are sensitive to the weather.

In West Africa, precipitation variability, defined as the mean deviation from the mean, is huge, sometimes reaching 40-80%, and increasing while annual precipitation totals are decreasing. In areas such as the Sahara Desert and the Sahel, where economic resources are limited, the

unpredictability of rainfall poses very serious threats to food security, and the lack of rainfall leads to localized and generalized food crises each year.

2.3. Climate change

Climate change refers to a statistically significant change in average climate status or variability, persisting for an extended period Sanda, 2009) Climate change is therefore a change in the state of the climate that can be identified by changes in the average and / or variability of its properties. This variability extends for long periods, usually decades or more.

Global warming is mainly caused by the emission of greenhouse gases. Indeed, they play an essential role in the regulation of the Earth's temperature. When the earth receives energy from the sun in the form of radiation, a part is reflected in the atmosphere by clouds or the surface of the earth. The rest is absorbed momentarily before being released as heat. The greenhouse gases then intervene to partially block the infrared rays, causing the increase of the average heat on the surface of the earth. Emissions of anthropogenic greenhouse gases increased significantly between 1970 and 2010, with a rising increase in recent decades.

Despite the introduction of more and more policies to reduce them, greenhouse gas emissions increased by 2.2% per year between 2000 and 2010; it is more than in the period 1970-2000, during which these emissions increased on average by 1.3% per year. Over the period evaluated by the IPCC (1970-2010), 78% of the increase in total greenhouse gas emissions can be attributed to the use of fossil fuels (coal, oil, gas for example) and industrial processes.

Africa is one of the most vulnerable continents to Climate Change in view of the strong demographic pressure (degradation of land and forests, dwindling water resources ...), weak infrastructure, extreme poverty, bad technology integration (IPCC 2007)

Added to this are recurrent conflicts, a notorious weakness in the management of health and a low capacity for adaptation.(Adama Alhassane DIALLO and Ibrah SEIDOU SANDA, 2009) .

As consequences of climate change, we can note, the warming of the climate system, the raising of the sea level, the melting of ice, the occurrence of extreme climatic phenomena, such as storms and droughts, the change of the rainfall regime. All these consequences have effects on health, agriculture, biodiversity, ecosystems, coasts and water resources.

In Africa, there are above average global temperature rises, a probable decrease in annual precipitation north of the Sahara and the Mediterranean zone and a probable increase in East Africa.

In Burkina Faso, where 80% of the population lives from agriculture, rainfall greatly affects the country's economy.

The analysis of the General Direction of Meteorology shows that the rainfall of Burkina Faso has changed during the twentieth century. The data observed during this period indicate a downward trend in annual rainfall totals over the entire country, a downward trend of the index over the number of rainy days and a trend of increasing numbers of consecutive days without rain PNA (2015) (plan national d'adaptation aux changements climatiques). The observation of extreme temperatures over the long term generally indicates an upward trend in hot days and hot nights, with the exception of the South-West regions where there is a downward trend on warm nights.

2.4. Climate scenarios (RCPs)

A climate scenario refers to a plausible future climate that has been constructed for explicit use in investigating the potential consequences of anthropogenic climate change. Such climate scenarios should represent future conditions that account for both human-induced climate change and natural climate variability.(T.R. Carter et al., 2001) Climate scenarios typically use climate projections, by manipulating model outputs and then combining them with observed climate data. A scenario is any reasonable or probable description of a future state of the world.

Representative Concentration Pathway (RCP) scenarios represent four radiative forcing path scenarios up to the 2300 horizon, which were established by the Intergovernmental Panel on Climate Change (IPCC) in its fifth report.

Previously, simulations were conducted in a linearly, i.e. greenhouse gas emission scenarios were first made using assumptions about demographic, social, economic and technological trends at the scale of the globe. So, climate projections represented the responses of numerical models to these emission scenarios.

As part of the Coupled Models Intercomparison Project-phase 5 (CMIP-5), climate modelers and economists worked in parallel which allow economists to develop scenarios that explore all the

potential for technological and socioeconomic change; also which take measures to reduce greenhouse gas emissions. Thus, climatologists produce climate projections using the RCP as input, while sociologists and economists develop scenarios leading, in output, on greenhouse gas emissions consistent with the RCP. In addition, the parallel approach does not require any new climate simulations after any modification of the socio-economic scenarios.

According to intensity of the radiative forcing there are RCP8.5, RCP6.0, RCP4.5 and RCP2.6 where RCP8.5 is the most severe corresponding to the pathway with the highest greenhouse gas emissions, and RCP2.6, the lower level, corresponding to virtuous behavior, very sober in emission of greenhouse gases.

Table 1: Main features of the four RCP scenarios

Name	Change in radiative balance (radiative forcing)	Concentration (in part per million)	Path
RCP8.5	> 8,5 W/m^2 in 2100	> 1370 eq- CO_2 in 2100	increasing
RCP6.0	~ 6 W/m^2 at stabilization level after 2100	~ 850 eq- CO_2 at stabilization level after 2100	Stabilization without exceeding
RCP4.5	~ 4,5 W/m^2 at stabilization level after 2100	~ 660 eq- CO_2 at stabilization level after 2100	Stabilization without exceeding
RCP2.6	Pic à ~ 3 W/m^2 before 2100 then decline	Pic ~ 490 eq- CO_2 before 2100 then decline	Peak then decline

2.5. The Climate models (GCM and RCM)

Climate models are based on well-established physical principles and have been demonstrated to reproduce observed features of recent climate and past climate changes. They represent fundamental physical processes in the atmosphere, ocean, land surface and cryosphere.

General Circulation Models (GCMs), are numerical models representing physical processes in the atmosphere, ocean, cryosphere and land surface, are the most advanced tools currently available for simulating the response of the global climate system to increasing greenhouse gas concentrations. GCMs have the potential to provide geographically and physically consistent estimates of regional climate change which are required in impact analysis (IPPC, 2013).

Regional Climate Model (RCM) is a climate model of higher spatial resolution than a GCM, providing more detailed simulations for a particular location. RCM uses data from more components of the regional climate system like atmosphere, land mostly but sometimes vegetation, snow, glaciers, hydrology, ocean, sea-ice, chemistry, aerosols, lake and human activities(Samuel Somot, 2012)**.**

2.6. CORDEX

CSAG's website provides details about the program CORDEX (refer to www.csag.uct.ac.za/cordex/ for more insights). The following summary heavily relies up on that source. CORDEX is an international project developed by the World Climate Research Program. It was birthed out of an increasing need for detailed, high-resolution regional information regarding future climate. CORDEX provides simulations from regional models (RCM), themselves forced by global models (GCM). CORDEX is organized into 14 domains each with their own GCM / RCM pairs. These GCM / RCM couples constitute a dynamic descent of scale which enables the projections to reach a relatively fine spatial resolution. The simulations applied to these GCM / RCM couples cover the four RCP scenarios ie RCP 2.6, RCP 4.5, RCP 6, and RCP 8.5. There are five main goals of the CORDEX programme. Firstly, it should provide a quality-controlled data set of regional scale climate information for the recent historical past and 21st century projections covering the majority of populated land regions on the globe. Secondly, it should define a common set of regions or domains for downscaling and define a standard set of variables, frequency and format for output and archival at a number of CORDEX data centres. The third goal is to coordinate a range of regional climate model simulations for the defined domains, forced by analyses of observations (currently the ERA-Interim reanalysis data) to provide a benchmark framework for model evaluation and assessment. The fourth goal is to encourage and coordinate the development of Regional Analysis and Evaluation Teams to evaluate the ensemble of downscaling, develop a suitable set of regionally-specific metrics for evaluation, collect suitable

observational data to evaluate high-resolution downscaling and design experiments to investigate the added-value of regional climate downscaling and target future priorities in this research. Fifth, CORDEX will permit to provide support and information to climate impact assessment and adaptation groups interested in utilizing

Table 2: Example of selection of climate change impact studies that used (not exclusively) CORDEX products *(adapted from Yira et al., 2017).*

Study	Location /size	GCM/RCM	Scenario	Reference period	Futur period	Precipitation change(%)	Discharge change (%)
Ruelland et al. (2012)	Bani catchment, Mali/100 000 km^2	MadCM3 et MPI-M	A2	1961–1990	2041–2070	-2 to -10	-30 to -46
Mbaye et al. (2015)	Upper Senegal Basin, Senegal–Mali–Mauritania/ 218 00 km^2	REMO-MPI-ESM-LR	RCP4.5 et RCP8.5	1971–2000	2071–2100	negative trend	up to -80
Aich et al. (2014)	Niger Basin/ 2 156 000 km^2	HadGEM2-ES, IPSL-5 CM5A-LR, MIROC-ESM-CHEM, GFDL-ESM2M, NorESM1-M	RCP8.5	1970–1999	2070–2099	mixed trend	-50 to +50
Ardoin-Bardin et al. (2009)	Sassandra, Ivory Coast/ 62 173 km^2	HadCM3-A2	-	1971–1995	2036–2065	11.4	38
Bossa et al. (2014)	Ouémé catchment, Benin/ 49 256 km^2	REMO-ECHAM5/ MPI-OM	A1B	2000–2009	2010–2029	-10	-18
Cornelissen et al. (2013)	Térou Catchment, Benin/2344 km^2	REMO-ECHAM5/ MPI-OM	B1	2001–2010	2031–2049	-11	-11
Kasei (2009)	Volta Basin/ 400 000 km^2	MM5 and REMO	B1	1991–2000 and 1961–2000	2030–2039 and 2001–2050	+12 and -6	+40 and –5
Yira et al. (2017)	Dano Catchment, Burkina Faso / 195 km^2	CCLM, RACMO22, HIRHAM5	RCP4.5 et RCP8.5	1971–2000	2021 to 2050	+3 to +50 and -15	-5 to -13 and +1 to +18

2.7. Hydrological cycle

The hydrological cycle is a natural phenomenon that represents the pathway between the large reservoirs of liquid, solid water or water vapor on Earth: the oceans, the atmosphere, the lakes, the rivers of water, groundwater and glaciers. The engine of this cycle is solar energy, which causes intense evaporation (Albergel and Braudeau, 1992).

Hydrological modeling

A hydrological model usually refers to the use of mathematical and logical expressions defining the existing relationships between flow characteristics (outputs) and its endogenous and exogenous conditional factors (inputs). They can broadly be classified into three groups: "empirical, conceptual, and physically based" (*Table 3*, Devia et al., 2015).

It is an essential tool in understanding watershed dynamics, in rational use of water resources in this basin, and in the fight against natural disasters associated with floods.(SOUSSOU SAMBOU et al., 2011) Hydrological models are used to quantify and assess water resources in such situations wich is critical to understanding the changes to water resources and to improve water resource management

It permits to analyze the impacts of the variability of precipitation on stocks and water flows in the different compartments of the water cycle at catchment scale. In addition, it takes into account the weight and spatial variability of other factors such as vegetation or soil (Laurent and Ruelland, 2010).

Table 3:characteristics of three groups of models (Devia et al., 2015)

Empirical model	Conceptual model	Physically based model
Data based or metric or black box model	Parametric or grey box model	Mechanistic or white box model
Involve mathematical equations , derive value from available time series	Based on modeling of reservoirs and Include semi empirical equations with a physical basis	Based on spatial distribution, Evaluation of parameters describing physical characteristics
Little consideration of features and processes of system	Parameters are derived from field data and calibration	Require data about initial state of model and morphology of catchment
High predictive power, low explanatory depth	Simple and can be easily implemented in computer code	Complex model. Require human expertise and computation capability
Cannot be generated to other catchments	Require large hydrological and meteorological data	Suffer from scale related problems

E.g: ANN, unit hydrograph	E.g: HBV model, TOPMODEL	E.g: SHE or MIKESHE model, SWAT
Valid within the boundary of given domain	Calibration involves curve fitting make difficult physical interpretation	Valid for wide range of situations.

2.8. Climate adaptation and mitigation

Adaptation means adapting to the climate change already in the pipeline while mitigation means reducing emissions of and stabilizing the levels of heat-trapping greenhouse gases in the atmosphere.

Adaptation involves adjusting to actual or expected future climate. The goal is to reduce our vulnerability to the harmful effects of climate change like sea-level encroachment, more intense extreme weather events or food insecurity. It also includes making the most of any potential beneficial opportunities associated with climate change, for example, longer growing seasons or increased yields in some regions.

Mitigation involves reducing the flow of heat-trapping greenhouse gases into the atmosphere, either by reducing sources of these gases, for example, the burning of fossil fuels for electricity, heat or transport, or enhancing the sinks that accumulate and store these gases such as the oceans, forests and soil. The goal of mitigation is to avoid significant human interference with the climate system, and "stabilize greenhouse gas levels in a timeframe sufficient to allow ecosystems to adapt naturally to climate change, ensure that food production is not threatened and to enable economic development to proceed in a sustainable manner" (from the 2014 report on Mitigation of Climate Change from the United Nations Intergovernmental Panel on Climate Change, page 4).

Chapter 3
METHODOLOGY

3.1. Study area

3.1.1. Location

The commune of Dano, capital of the Province of IOBA, is located in the South-West Region of Burkina Faso and covers an area of approximately 195 km2 (Figure 1). It is bounded by the commune of Koper in the East, the Communes of Guéguéré and Dissin in the West, the commune of Koti in the North, the commune of Fara in the North-East and the commune of Oronkua in the North-West. The city of Dano is divided into 7 sectors of which only one fully subdivided (sector 4), three partially divided sectors (sectors 1, 2, 3) and three others completely unbaked (sectors 5, 6 and 7) with 24 villages attached.

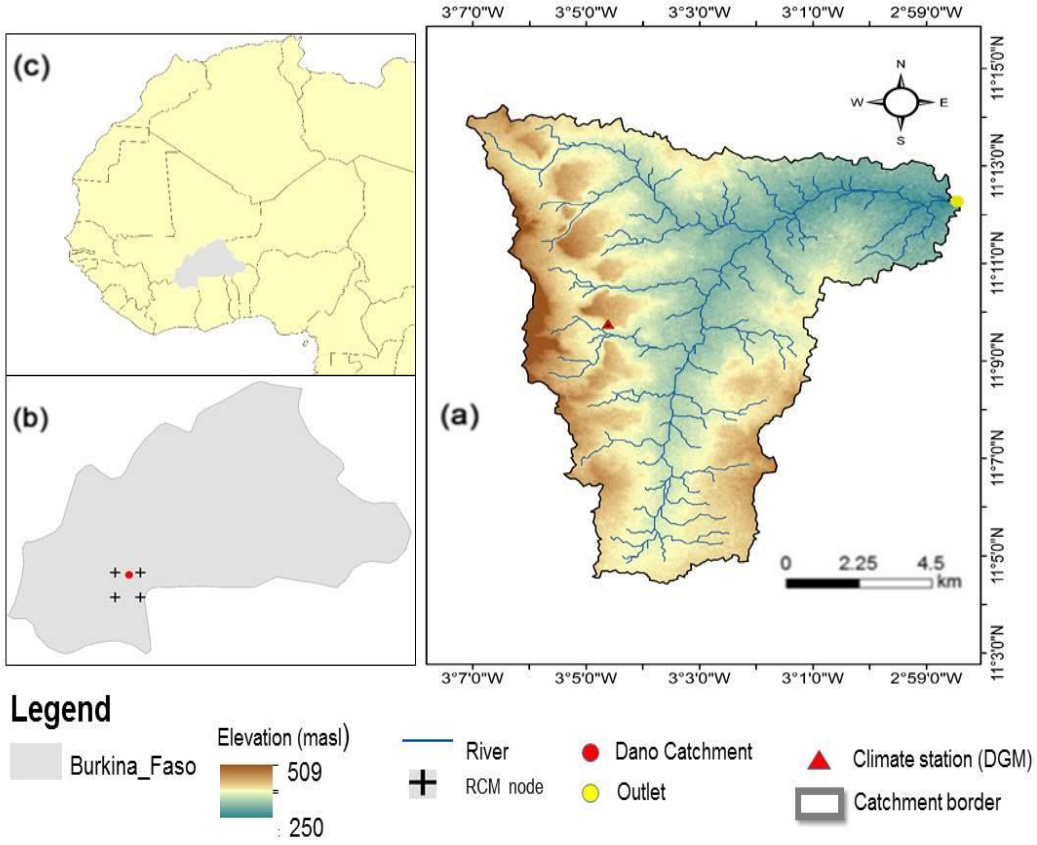

Figure 1: a-Location map; b-Dano catchment in Burkina-Faso; c-West Africa.

3.1.2. Climate

Located in the Sudanese climate zone, the municipality of Dano is characterized by the alternation of two seasons including a dry season of 6 to 7 months (November to April) and a rainy

season of 5 months (May to October) (*Figure 2*). The climate regime is regulated by the oscillation of the intertropical convergence zone front (ITCZ), which is controlled by the Sahara anticyclone and that of the southern hemisphere (Sivakumar and Faustin Gnoumou, 1987).

Average annual temperatures are around 27 ° C for average monthly temperatures between 24 ° C and 32 ° C with an average annual rainfall over the last 10 years of 958 mm (Figure x). An average of + 0.31 ° C / decade and + 0.17 ° C / decade, respectively for minimum and maximum temperature, is reported for the region taking into account the period 1960-2010 (Waongo et al., 2015).

The hottest month of the year is April with an average temperature of 30.9 ° C while the coldest is August with an average temperature of 25.7 ° C. The difference in precipitation between the driest month and the wettest month is 253 mm. Annual precipitation ranged from 800 mm to 1200 mm for the period 1951 to 2005(Schmengler, 2011).

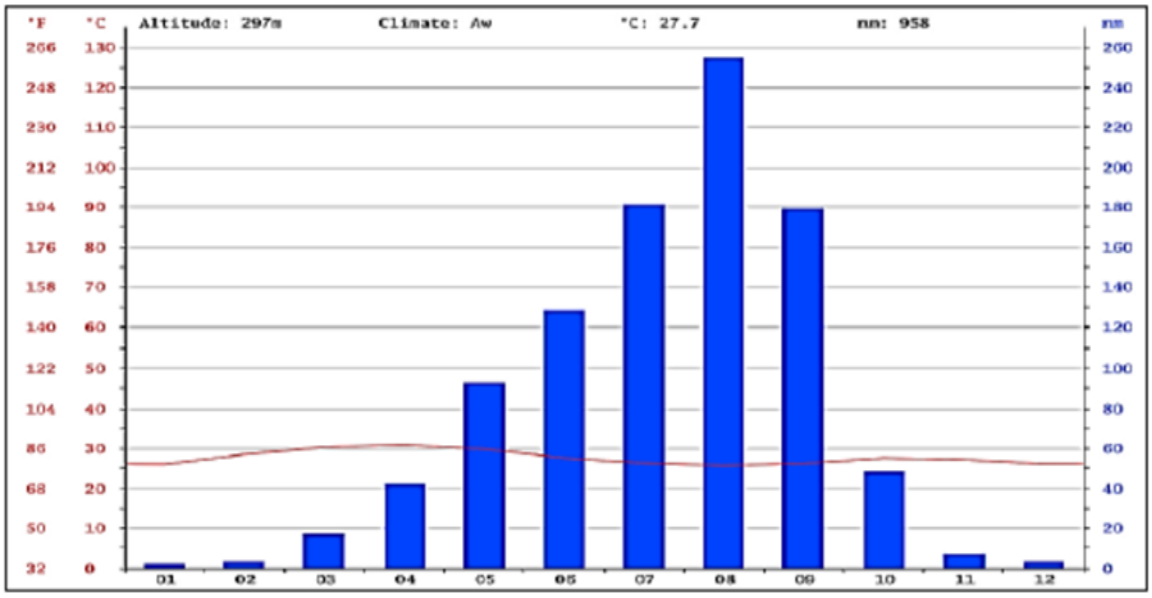

Figure 2: Climat graph of Dano city (http://climate-data.org/)

3.1.3. Hydrology

Several streams are drained into the watershed. However, these rivers dry up in the dry season. The river regime is governed by the ITCZ front. Storms recorded during the rainy season cause runoff (for the period from June to October). The presence of groundwater in the area would be associated with the development of secondary porosity, such as joints, fractures, shears and

cracks. As a result, aquifer systems in the watershed would be highly discontinuous with individual compartments in which isolated groundwater circulation occurs (Amisigo B. A. and van de Giesen N. C., 2005).

3.1.4. Soils

The city of Dano is located in a basin made up of lateritic mounds battleships. It is based on a very extensive granite massif and covers most of the built-up area of the city. However, some lateritic gravels with high permeabilities (in accessible areas) and an indurated lateritic armor section that cannot be pierced with a pickaxe and is likely to be impermeable are observed. The very rugged terrain facilitates soil erosion through very fast runoff. The main types of soils encountered are (Monographie de la commune de Dano, avril 2006) PSA-DANO (2017):

- Soils of gravels (Wora) in a state of continuous degradation: These sandy soils at the surface and deep sandy-clay, occupy nearly 18% of the urban area and are concentrated in sectors 2 and 3. They are conducive to the cultivation of peanuts, beans (cowpeas) and millet.
- The eutrophic brown soils on clay materials derived from basic rocks (Gbaan): they are sandy-loamy on the surface and clayey in depth. They are characterized by a high biological activity humus, a good structure, a high calcium saturation complex and a reddish-brown color in the B horizon. Spread over about 14% of the city's surface, they are concentrate at sector level 1. Satisfactory fertility because they are rich in organic matter, they are suitable for the production of maize, beans, millet, cotton, peanuts, etc.

  The ferruginous soils leached (Dalempouo): sometimes gravelly shale, these soils are characterized by their high content of oxides and hydroxides of iron or manganese which gives them a red, ocher or black color. They are low in organic matter and occupy a large part of the city's surface, about 69%. They are sandy on the surface, clayey in depth and then of low permeability and porosity. They occur in sectors 3, 4, 5, 6 and in part of sector 7. There is another category of soils, called hydromorphic soils, which are found mainly around rivers. They occupy about 5% of the urban area and are suitable for rice growing and gardening.

3.1.5. Vegetation

The Dano watershed is part of the Sudanese phytogeographic domain which is the savannah and forest area (Boussim, 2010). The natural vegetation of this sector is characterized by:

- A herbaceous layer composed of *Andropogon pseudapricus*, *Elionurus elegans*, *Loudetia togoensis*, *Pennisetum pedicellatum*, *Schizachyrium exile*, *Aristida adsenscionis*, *Cenchrus biflorus*, *Ctenium elegans*, *Cymbopogon schoenanthus*, *Schoenefeldia gracilis*, etc.
- Tree species dominated *by Faidherbia albida*, *Lannea microcarpa*, *Parkia biglobosa*, *Tamarindus indica*, *Vitellaria paradoxa*, *Acacia erythrocalyx*, *Anogeissus leiocarpa*, *Celtis integrifolia*, *Diospyros mespiliformis*, *Pterocarpus erinaceus*, etc.
- Most of the primary vegetation has been converted to agriculture and long-term fallow in recent decades. The main crops are: Sorghum bicolor (sorghum), Gossypium hirsutum (cotton), Zea mays (maize), Pennisetum glaucum (millet), Oryza sativa and Oryza glaberrima (rice, produced in the interior valleys), Vigna unguiculata (cowpea, often associated with sorghum), Arachis hypogaea (peanut) and Sesamum indicum (sesame).
- A special feature of Dano (and the southwestern part of the country) is the intensive use of firewood to produce local beer called "dolo". About 6,442 tonnes of wood are used each year for the production of this local drink (Fotseu et al., 2012), thus constituting an additional factor of degradation of natural vegetation.

3.1.7. Population

The population of the city of Dano was 17,068 in 2006 according to the General Population and Housing Census (RGPH). With a provincial population growth rate of 4.8%, the population of the urban center of Dano is estimated at 28,586 in 2017. Like most localities in the country, the economy is essentially based on the agriculture sector with a very diversified agricultural production. This activity employs about 86% of the population and is distributed on the one hand in food crops, and on the other hand in market gardening (intensified in recent years) and cash crops. With regard to food production, traditional agriculture is practiced on a single period of the

year (rainy season), with rudimentary production techniques. According to Ki (2008) there is extensive subsistence farming (farmers expanding their acreage to increase their production), but with low yields.

In addition to agricultural activities, women are particularly active in gathering fruit and firewood, petty trade, handicrafts and food trade (Callo-Concha et al., 2012).

For the commune as a whole, production increased by 90.4% from 2003 to 2005, from 195.4 tonnes to 372.05 tonnes. The area sown for all speculations increased by 20.35% between 2002 and 2004, rising from 11,421.75 ha to 13,745.8 ha. At the level of market gardening, the evolution is clearly perceptible. In the monograph of Dano (2006), the areas planted had doubled in 2 years (from 2003 to 2005). Market gardening is largely practiced around the lowlands of Lofing village, the Moutori dam and the impoundment of the village of Pontiéba. Off-season activities provide additional income for producers.

In addition, the rate of access to drinking water in rural areas is about 63% (MEAHA, 2013). As a result, a very large part of the population is heavily dependent on surface water as a source of supply.

3.2. **Materials and methods**

3.2.2. Modeling approach (Model description, calibration and validation)

A quantitative analysis of climate changes impact on water resources in a hydrological system requires simulation models that adequately represent the system features. The study adopted a multi-model approach combing two conceptual hydrological models HBV-light and GR4J, both publicly available.

3.2.2.1. HBV-light

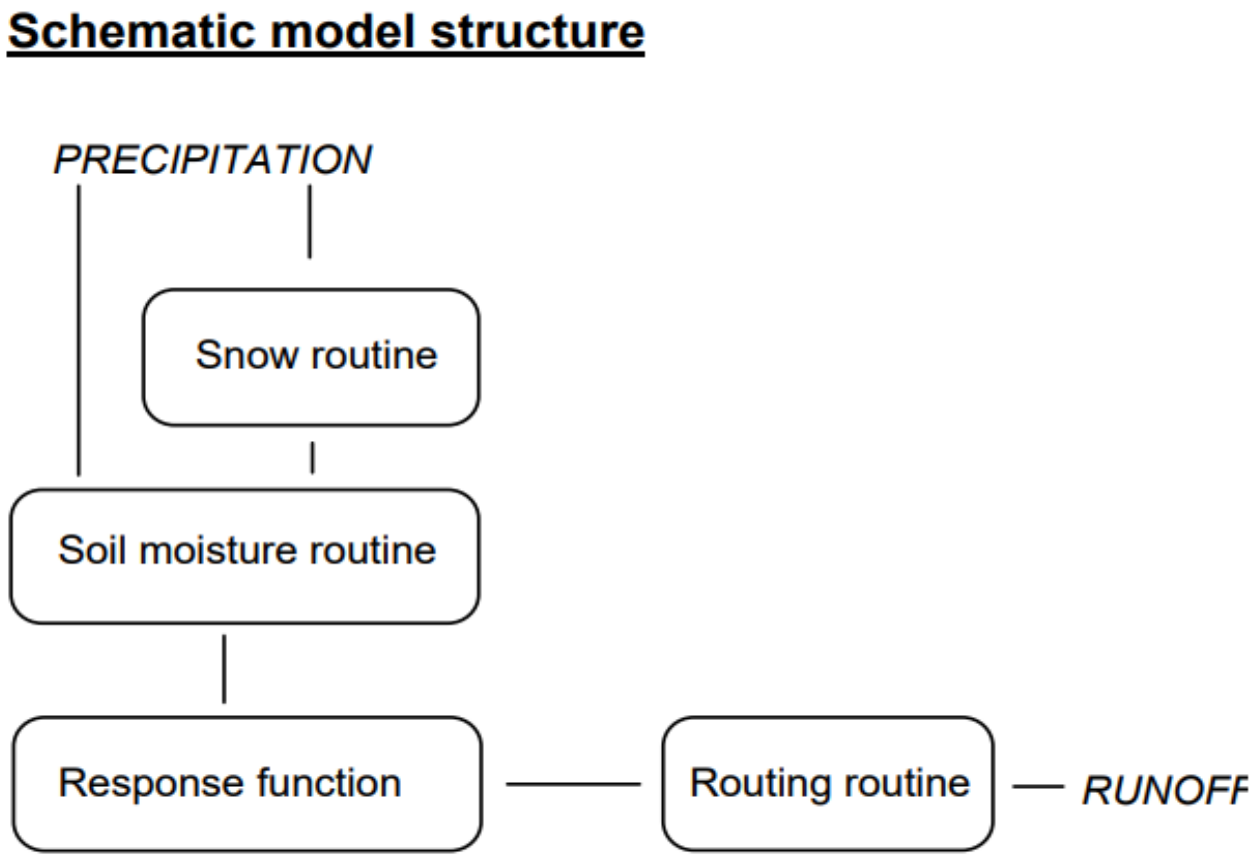

Figure *3*: Schematic structure of the HBV model

HBV-light has been developed at Uppsala University (and further improved at Oregon State University, SLU-Uppsala and Stockholm University) by Jan Seibert. The model simulates daily discharge using daily rainfall, temperature and potential evaporation as input. Precipitation is simulated to be either snow or rain depending on whether the temperature is above or below a threshold temperature, TT [°C]. All precipitation simulated to be snow, i.e. falling when the temperature is bellow TT, is multiplied by a snowfall correction factor, SFCF [-]. Snowmelt is calculated with the degree-day method (Equation 1). Meltwater and rainfall is retained within the snowpack until it exceeds a certain fraction, CWH [-], of the water equivalent of the snow. Liquid water within the snowpack refreezes according to Equation 2. It is worth mentioning that the snow component is not applicable to the current modeling exercise due to climate conditions of the investigation area (see section ?? for the climate of the Dano catchment). Rainfall (P) is divided into water filling the soil box and groundwater recharge depending on the relation between water

content of the soil box (SM [mm]) and its largest value (FC [mm]) (Equation 3). Actual evaporation from the soil box equals the potential evaporation if SM/FC is above *LP* [-] while a linear reduction is used when SM/FC is below LP (Equation 4). Groundwater recharge is added to the upper groundwater box (SUZ [mm]). PERC [mm d^{-1}] defines the maximum percolation rate from the upper to the lower groundwater box (SLZ [mm]). Runoff from the groundwater boxes is computed as the sum of two or three linear outflow equations depending on whether SUZ is above a threshold value, UZL [mm], or not (Equation 5). This runoff is finally transformed by a triangular weighting function defined by the parameter *MAXBAS* (Equation 6) to give the simulated runoff [mm d^{-1}].

If different elevation zones are used the changes precipitation and temperature with elevation are calculated using the two parameters PCALT [%/100 m] and TCALT [ºC / 100 m] (Equation 7 and 8). This feature was however not applied.

The long-term mean of the potential evaporation, $E_{pot,\,M}$ for a certain day of the year can be corrected to its value at day t $E_{pot(t)}$, by using the deviations of the temperature, T(t), from its long-term mean, TM, and a correction factor, CET [$°C^{-1}$] (Equation 9).
Please note that more information can be found in Part 2.

melt = CFMAX (T(t) - TT) (1)

refreezing CFR CFMAX *(*TT-T*(*t)) (2)

$$\frac{recharge}{P(t)} = (\frac{SM(t)}{FC})\text{^}Beta \quad (3)$$

$$Eact = Epot \min(\frac{SM(t)}{FC-LP}, 1) \quad (4)$$

Q_{GW} (t) = K_2SLZ + K_1SUZ + K_o max (SUZ – UZL, 0) (5)

$$\text{Qsim } (t) = \sum_{i=1}^{MAXBAS} C(i) QGW\ (t-i+1)$$

$$\text{Where } C(i) = \int_{i-1}^{i} \frac{2}{MAXBAS} - \left|U - \frac{MAXBAS}{2}\right| * \frac{4}{MAXBAS^2}\, du \quad (6)$$

$$P(h) = P0\ (1 + PCALT\ (h - h0)/10000) \quad (7)$$

$$T(h) = T0 - TCALT\ (h - h0)/100 \quad (8)$$

$$Epot\ (t) = \ (1 + C_{ET}\ \left(T_{(t)} - T_M\right))E_{pot,M} \quad (9)$$

But $0 \leq E_{POT(t)} \leq 2\, E_{POt,M}$

3.2.2.2. Model description GR4J

The GR4J model is a global rain-flow model with four parameters. Its development has been initiated at Cemagref in the early 1980s, with the aim of developing a robust and reliable rain-flow simulation model for use in applications water resources management and engineering (design of structures, forecasting of floods and low flows, reservoir management, impact detection ...)

This model has known several versions, proposed successively by Edijatno and Michel (1989), Edijatno (1991), Nascimento (1995), Edijatno et al. (1999), Perrin (2000), Perrin (2002) and Perrin et al. (2003), which have gradually improved the performance of the model. This is the version of Perrin et al. (2003) which is presented here.

Although GR4J is an empirical model, its structure is similar to conceptual models tanks, with a procedure for monitoring the state of humidity of the basin that allows to hold account of previous conditions and to ensure their continued operation. Its structure combines a production function and a transfer function (associated with a reservoir of routing, to a unit hydrograph with a possibility of exchange with the outside of the basin) to simulate the hydrological behavior of a basin.

Mathematical description

A diagram of the structure is given in Figure 4. *Pk* is the daily rain of the day k and E.

Potential average evapotranspiration for the same calendar day.

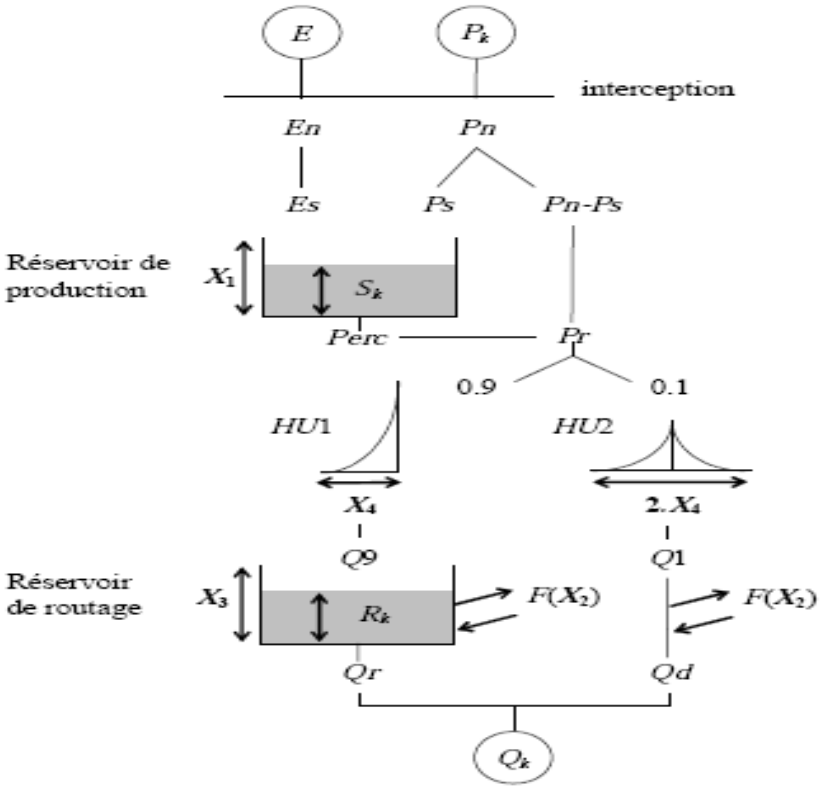

Figure 4: the structure of the hydrological model GR4J

- ***Neutralization***

The first operation is the neutralization of Pk by E to determine a net rain Pn

a net evapotranspiration calculated by:

If Pk= E, then Pn = Pk - E and En = 0

If Pk=E, then Pn=0 and En = E- Pk

- **Performance function**

In the case where Pn is different from zero, a part Ps of Pn feeds the reservoir of production and is calculated by:

$$P_n = \frac{X1 * \left(1 - \left(\frac{SK}{X1}\right)^2\right) * \tanh\left(\frac{P_n}{X1}\right)}{1 + \frac{SK}{X1} * \tanh\left(\frac{P_n}{X1}\right)}$$

Where: X1 (mm) is the maximum capacity of the production tank and Sk the contents of the production tank at the beginning of the day k

In the opposite case, when Pn is zero, an evaporation amount Es is removed from the

production tank. It is given by:

$$E_S = \frac{SK * \left(2 - \frac{SK}{X1}\right) * tanh\left(\frac{E_n}{X1}\right)}{1 + (1 + SK/X1) * \tanh(\frac{En}{X1})}$$

The content of the reservoir resulting from these operations is given by:

$\boldsymbol{S'} = \boldsymbol{Sk} + \boldsymbol{Ps} - \boldsymbol{Es}$

- **Percolation**

A percolation Perc resulting from the production tank is then calculated by the following equation:

$$\boldsymbol{Persc} = \boldsymbol{S'} * \left(\mathbf{1} - \left[\mathbf{1} + \left(\frac{\mathbf{4}}{\mathbf{9}}\frac{\boldsymbol{S'}}{\boldsymbol{X1}}\right)^{\mathbf{4}}\right]^{\mathbf{-1/4}}\right)$$

As a result, the contents of the tank becomes

$$\boldsymbol{Sk} + \mathbf{1} = \boldsymbol{S'} - \boldsymbol{Perc}$$

And the amount of water for who ultimately reaches the routing part of the model is given by:

$$\boldsymbol{Pr} = \boldsymbol{Perc} + (\boldsymbol{Pn} - \boldsymbol{Ps})$$

- **Unit hydrographs**

Pr is divided into two flow components, 90% being routed by a HU1 unit hydrograph and a routing reservoir and 10% by a symmetric HU2 unit hydrograph. HU1 and HU2 depend on the same parameter X4, base time of HU1 expressed in days. The ordinates of the hydrographs are calculated from the S curves respectively denoted SH1 and SH2, which correspond to the cumulative functions of the hydrograph.SH1 is defined as a function of time by:

For $\boldsymbol{t \leq 0, SH1(t) = 0}$

Four $\boldsymbol{0 \leq t \leq X4}$, $\boldsymbol{SH1(t)} = \left(\frac{t}{X4}\right)^{5/2}$

For $\boldsymbol{t \geq X4,\ SH1(t) = 1}$

For $\boldsymbol{t \leq 0, SH2(t) = 0}$

For $\boldsymbol{0 \leq t \leq X4,\ SH2(t) = \frac{1}{2}\left(\left(\frac{t}{X4}\right)^{5/2}\right)}$

For $\boldsymbol{X4 \leq t \leq 2X4,\ SH2(t) = 1 - \frac{1}{2}\left(2 - \frac{t}{X4}\right)^{5/2}}$

For $\boldsymbol{t \geq 2X4,\ SH2(t) = 1}$

The ordinates of HU1 and HU2 are then calculated by:

$$\boldsymbol{UH1(j) = SH1(j) - SH1(j-1)}$$

$$\boldsymbol{UH2(j) = SH2(j) - SH2(j-1)}$$ where j is an integer.

At each time step k, the outputs Q9 and Q1 of the two hydrographs correspond to the convolution of the previous rains by the distribution key given by the discrete hydrograph and are calculated by:

$$\boldsymbol{Q9(k) = 0.9 * \sum_{j=1}^{l} UH1(j) * Pr(k-j+1)}$$

$$\boldsymbol{Q1(k) = 0.1 * \sum_{j=1}^{m} UH2(j) * Pr(k-j+1)}$$

Where l= int(X4)+1 and m= int(2X4)+1, int() designating the entire part.

- **Exchange function with non-atmospheric exterior**

An underground water exchange is calculated by:

$$\boldsymbol{F = X2 * \left(\frac{Rk}{X3}\right)^{7/2}}$$

Where: Rk is the level in the tank at the beginning of time step, X3 the capacity at a day of the reservoir and X2 the water exchange coefficient which can be positive in the case of contributions,

negative in the case of losses to deep layers or none. In fact, the physical interpretation of this exchange function is not direct.

- **Routing tank**

The level in the routing tank is modified by adding the Q9 output of hydrograph HU1 and F.

$$\boldsymbol{R' = max(0; Rk + Q9(k) + F}$$

It then empties into an output Qr given by

$$\boldsymbol{Qr = R' * \left(1 - \left[1 + \left(\frac{R'}{X3}\right)^4\right]^{-1/4}\right)}$$

The level in the tank becomes:

$$\boldsymbol{Rk + 1 = R' - Qr}$$

- **Total flow**

The output Q1 of the hydrograph HU2 is subjected to the same exchange to give the

flow component Qd:

$$\boldsymbol{Qd = max(0; Q1(k) + F)}$$

Le débit total Qk est alors donné par :

$$\boldsymbol{Qk = Qr + Qd}$$

The GR4J model has only four parameters to stall:

X1: capacity of the production tank (mm)

X2: underground trade coefficient (mm)

X3: one-day capacity of the routing tank (mm)

X4: base time of unit hydrogram HU1 (j)

- **Calibration and Model Fit Criteria (Objective Function)**

Calibration is the phase in which the model's parameter set is optimized. To optimize, an algorithm is generally used. In the current study, the built-in Genetic Algorithm and Powell optimization (GAP) Seibert (2000) and the Solver of MS-Excel were used for the calibration and validation of HBV-light and GR4J, respectively.

The adjustment criterion or objective function makes it possible to measure the relevance of the model by comparing observed flow rates with simulated flow rates. The Nash criterion (Nash and Sutcliffe, 1970) and the Coefficient of Determination R^2 were used.

- **The Nash criterion -NSE**

A null Nash means that the simulation is equivalent to the reference model used. If the criterion takes a value close to 1, the simulated flows are close to the observed flow rates.

$$\boldsymbol{NSE} = \left[\mathbf{1} - \frac{\sum(\boldsymbol{Q0}, \boldsymbol{i} - \boldsymbol{Qm}, \boldsymbol{i})^{\mathbf{2}}}{\sum(\boldsymbol{Q0}, \boldsymbol{i} - \boldsymbol{Q0})^{\mathbf{2}}}\right]$$

NSE is sensitive to strong flows. In practice, studies have considered that Nash is acceptable from the value 0.6 (NASH and SUTCLIFF, 1970, O'CONNELL et al., 1970). Based on these considerations, it will be assumed that the simulation is of poor quality when the Nash criterion is low (<0.6), it is acceptable when it is between 0.60 and 0.80 and perfect when it is greater than 0.90.

- **The coefficient of determination - R^2**

$$R^2 = \frac{\sum_{i=1}^{n} (Q_{i,calc} - \overline{Q}_{obs})^2}{\sum_{1=1}^{n} (Q_{i,obs} - \overline{Q}_{obs})^2}$$

The value of R^2 describes the proportion of the variance of the observed flow rates compared to the simulated flow rates. Authors such as Moriasi D. N et al. (2007) suggest that any R^2 value greater than 0.5 for daily flow comparisons is an acceptable threshold for hydrological simulation.

3.2.3. Input and data sources

- **Climate (observation, simulation CORDEX data)**

The hydroclimatic data (Rain, ETP, Temperatures, solar radiation, wind speed) for calibration and validation of the model in this study come from the database of the WASCAL competence center. They cover the period from 2012 to 2016. In addition, data for climatic simulation come from CORDEX's database and cover the period from 1956 to 2005, for historical data, and the period from 2006 to 2100, for projected scenarios.

An ensemble of five RCM–GCM datasets is exploited in the study: HadGEM2-ES-CCLM, HadGEM2-ES-RCA, ESM-CCLM, ESM-REMO and ESM-RCA. The RCM–GCM simulations were performed in the framework of the CORDEX-Africa project.

To simulate the catchment's climate, an extent of 4 nodes of CORDEX-Africa domain was delineated. The climate historical and projected variables of the extent of 4 nodes (average) were used as inputs for the hydrological simulation models.

The raw outputs of climate models often have disadvantages. (e.g. biases due to an imperfect representation of physical phenomena). Bias correction if therefore often used to reduce the discrepancies between observed and simulated (historical) data. However, a consistent application of bias correction is subject to numerous hypotheses that need to be fulfilled, at the risk of altering the climate change signal (Muerth et al., 2013; Ehret et al., 2012; Hagemann et al., 2011). The fulfillment of these conditions goes beyond the scope of the current study. Furthermore, having bias corrected data, does not shirk the obligation of presenting the results achieved with non-bias corrected data. Therefore, the study applied non-bias corrected climate data for both climate change signal detection and hydrological impact assessment. .Matlab was used to extract the data of the 4 nodes surrounding the Dano catchment as the native format of CORDEX data (NetCDF) is not directly applicable as input to the HBV-light and GR4J models.

The data of the extracted 4 nodes were averaged and used as climate input for the hydrological simulation model. Therefore, for each period (historical and projected scenarios) a simulation corresponding to the averaged four nodes are performed per RCM–GCM.

- **Discharge**

The flow data for calibration and model validation in this study comes from the WASCAL Competence Center database. They come from the Batiara Station in the Dano Basin. They cover the period 2013-2016.

In addition, the period considers for calibration and validation spans from 2012 to 2016 but the flow data starts from 10/02/2013. The period from 2012 to 10/01/2013, where flow data are missing, was considered for the period of the start of the model (warm up phase).

- **Impact assessment**

In this study the assessment of climate change will be done following the difference between models (HBV-light and GR4J) outputs for the projected periods and the historical one.

Projections forced by the RCP4.5 scenarios were used. For each pair of models (GCM / RCM), the "historical" data covers the period of 1976-2005 while two future periods are considered:2021-2050 (mid-century) and 2071-2100(end of the century).

Chapter 4:

RESULTS AND DISCUSSION

4.1. Results

4.1.1. Hydrological model's calibration and validation

Error! Reference source not found. shows the simulated and observed discharges for the calibration period (10/02 / 2013-31 / 12/2015) for the HBV-light hydrological model. Satisfactory results are obtained as shown by the model statistical quality measures of NSE criteria of 0.73 and R2 of 0.77. However, peak flows are underestimated by the model throughout the calibration period. This could be explained by the uncertainty associated with peak flow measurements as peak flows in the catchment are characterized by over bank flow.

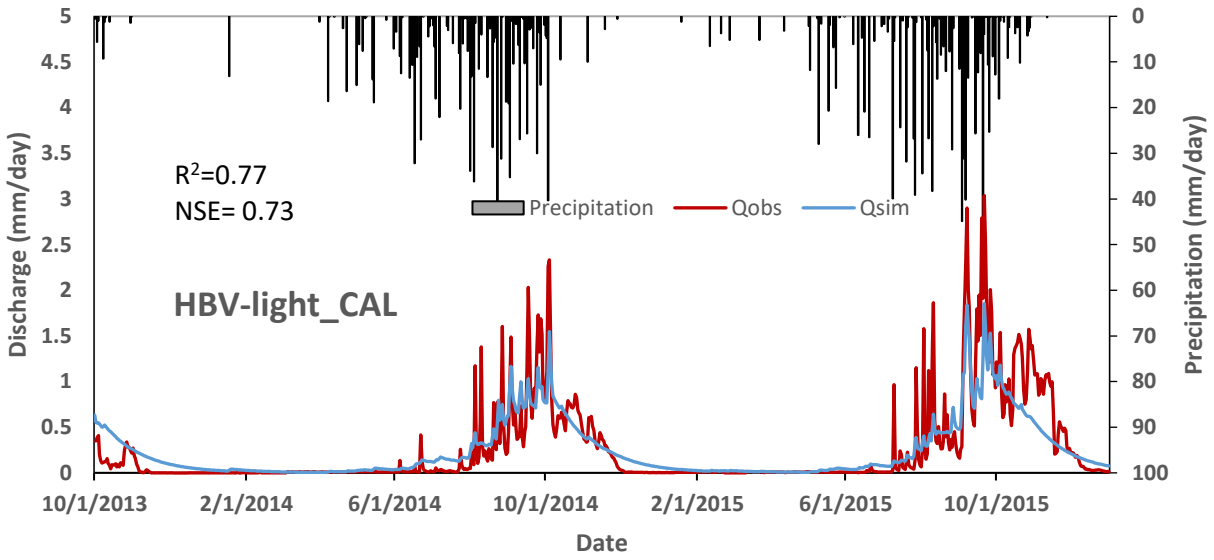

Figure 4:Comparison between observed and simulated discharge for the calibration period (2013-2015) using the HBV-light model

Following the satisfactory calibration result, the HBV-light hydrological model was validated with a Nash = 0.85 and R^2 = 0.88. The 2016 period was considered for this validation (Figure 5*:Comparison between observed and simulated discharges for the calibration period (2013-2015) using the HBV-light model*

Figure 6). The model shows higher performances in view of the Nash and R2 values and thus testifying its ability to simulate the hydrological regime of the catchment.

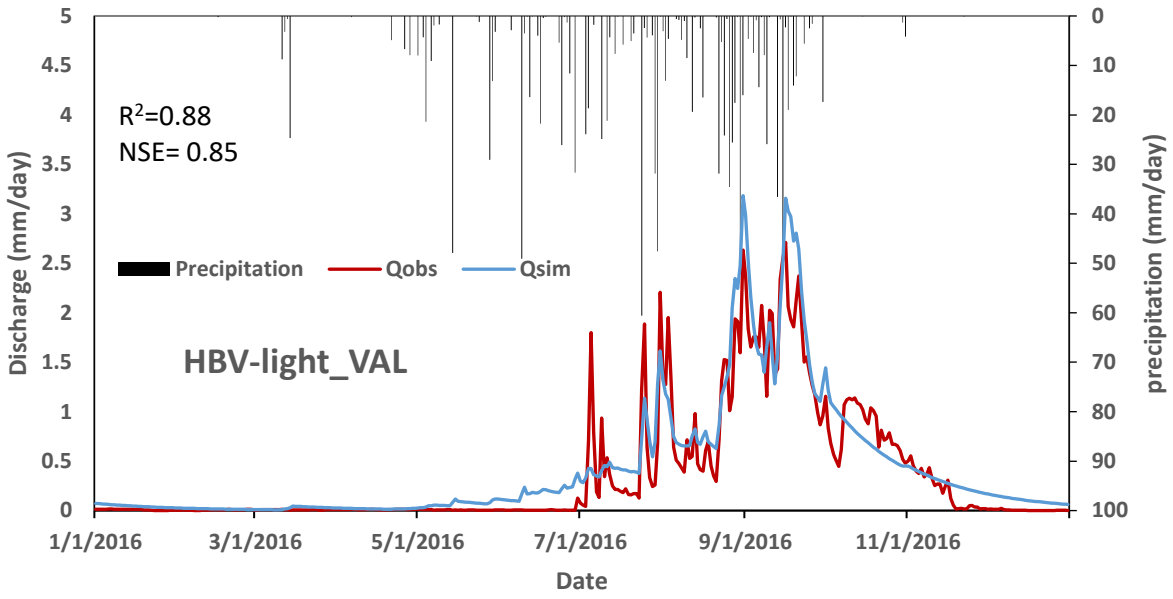

Figure 5:Comparison between observed and simulated discharges for the calibration period (2013-2015) using the HBV-light model

Figure 6 shows the simulated and observed discharges for the calibration of the GR4J hydrological model for period 10/02 / 2013-31 / 12/2015. As for HBV-light, satisfactory results are also obtained as shown by the goodness fit criteria's of NSE criteria of 0.64 and R2 of 0.73. peak flows are also underestimated by the model throughout the calibration period. As both models use the same observation data as input, the uncertainty associated with the observed discharge for peak flows applies as well.

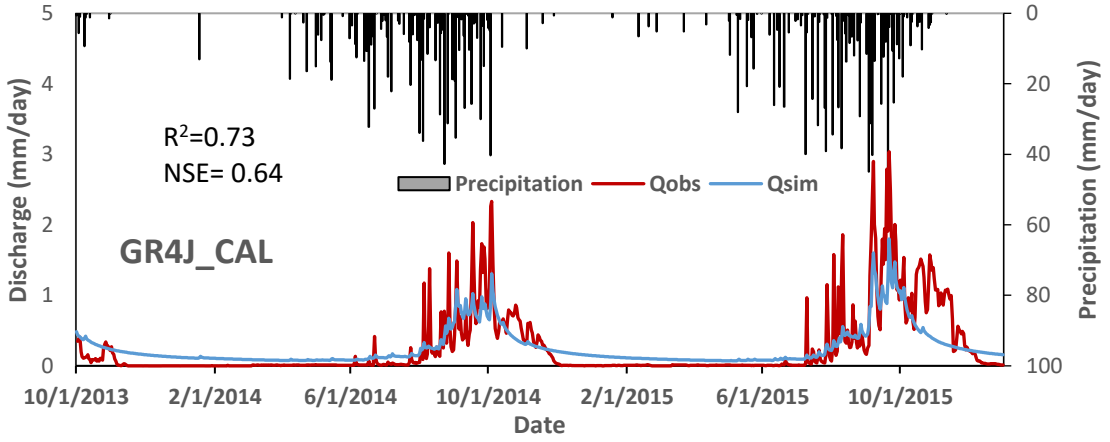

Figure 6: Comparison between observed and simulated discharges for the calibration period (2013-2015) using the GR4J hydrological model

The satisfactory calibration of the GR4J hydrological model allowed the validation of the model with a Nash = 0.80 and R^2 = 0.83. the 2016 period was considered for this validation (**Error! Reference source not found.**). The model shows improved performances in view of the Nash and R2 values and thus testifying a good ability to reproduce the discharge of the catchment.

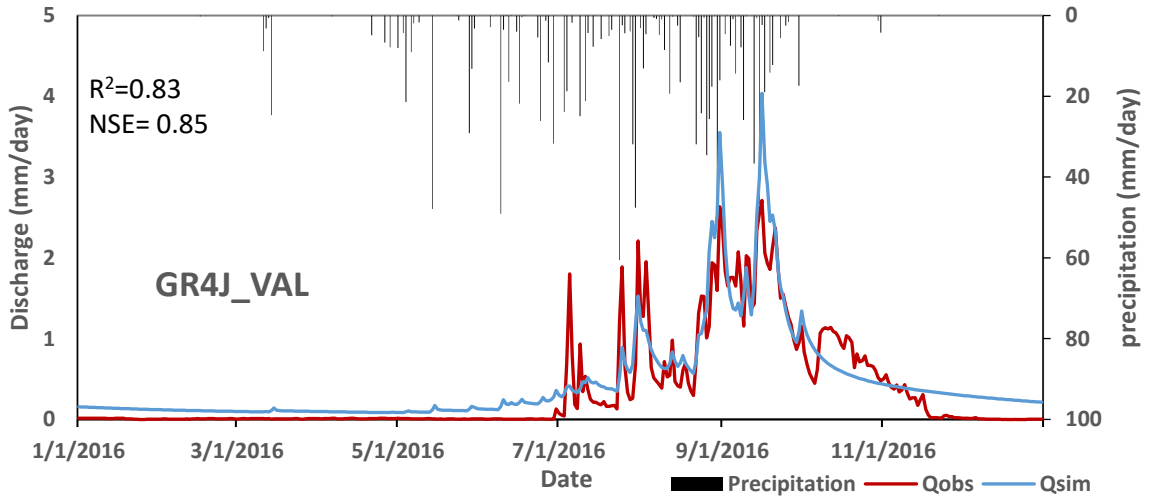

Figure 7: Comparison between observed and simulated discharges for the validation period (2013-2015) using the GR4J hydrological model

4.1.2. Climate change signal of the Dano catchment (Precipitation and ETp)

Figure 8: Comparison between the historical (1976-2005) and projected (2021-2050 and 2071-2100) mean annual rainfall pattern of five climate models.

Figure 9 shows historical precipitation (1976-2005) and projections (2021-2050 and 2071-2100). For the set of climatic products (HadGEM2-CCLM, HadGEM2-RCA, ESM-CCLM, ESM-RCA, ESM-REMO), we notice that the rain generally starts between March and April and stops in November and the maximum rainfall is recorded between August and September. This is valid for both the historical and future periods. For HadGEM2-CCLM and HadGEM2-RCA the maximum rainfall is around 200 mm for the historical period and projections. While for ESM-CCLM, ESM-RCA and ESM-REMO the maximum rainfall is greater than 300 mm for the historical period (1976-2050) and projection 1 (2021-2050) and 300 mm turn for P2 projection (2071-2100) for the ESM-REMO product. For ESM-CCLM product, the maximum rainfall is 300 mm for the projection 1, 270 mm for the P2 projection and 200 mm for the historical period. For ESM-RCA the maximum rainfall is 240 mm turn for the historical period, 200 mm for the projection and 180 mm P2 projection. The projected maximum monthly rainfall thus shows both increasing and decreasing trends depending on the considered regional climate model.

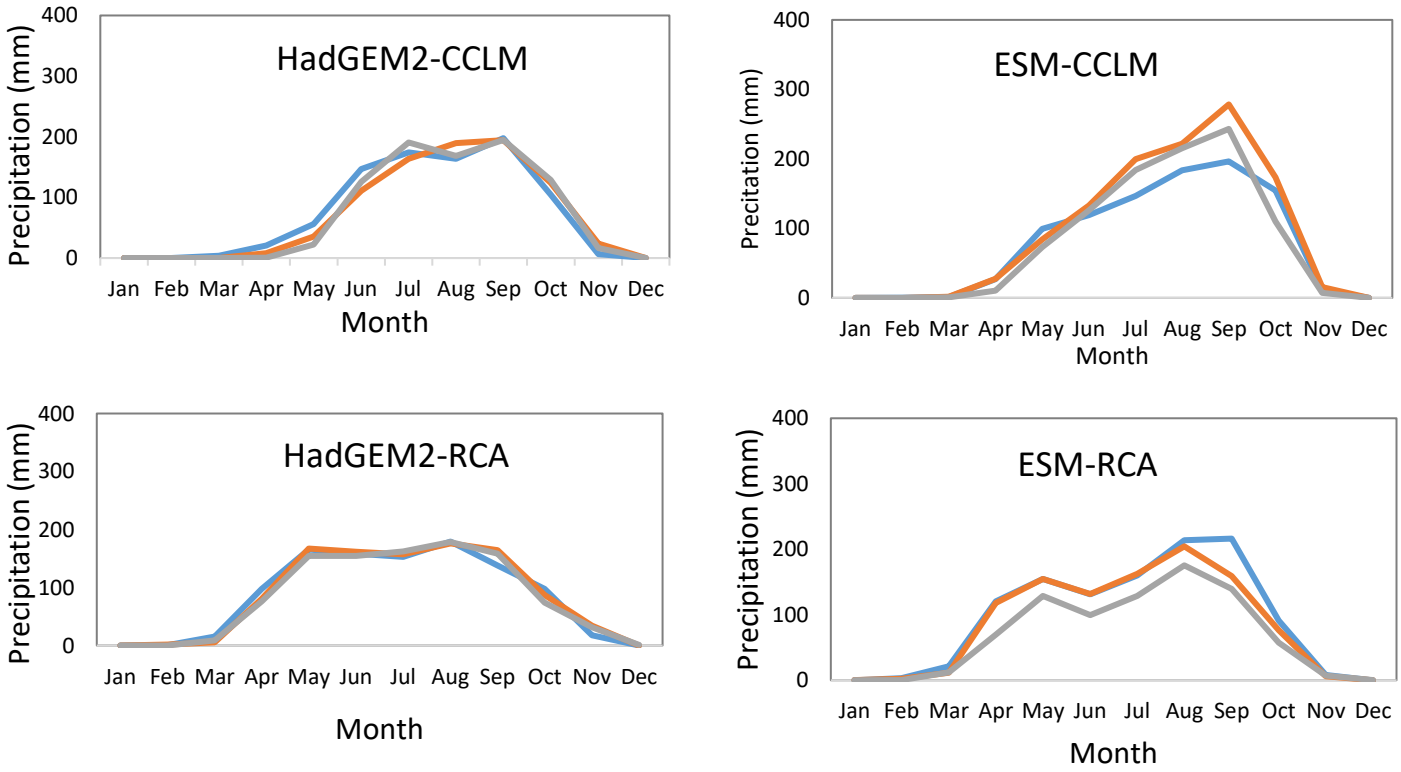

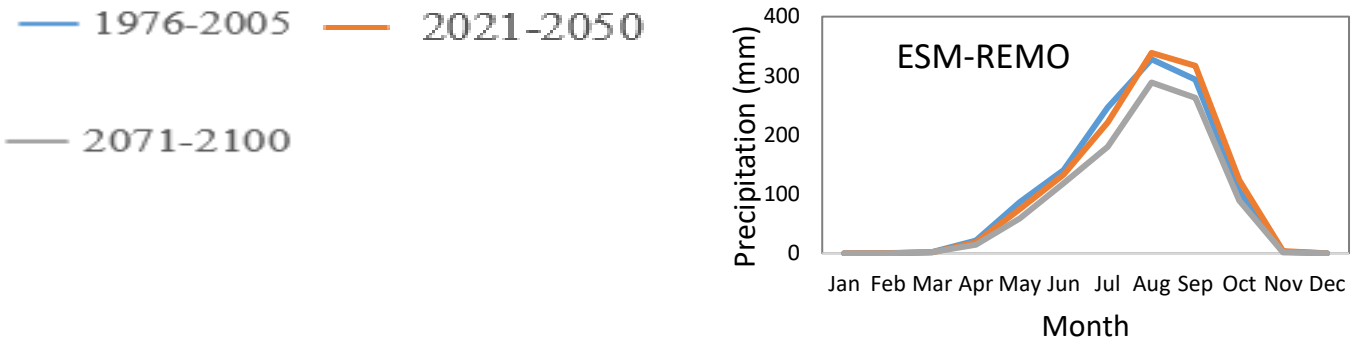

Figure 8: Comparison between the historical (1976-2005) and projected (2021-2050 and 2071-2100) mean annual rainfall pattern of five climate models.

Figure 9 shows the precipitation diagram presenting different situation according to climate models.For the HadGEM2-CCLM one observes an increase of rains in August for the P2 & P1 projections. There is a balance between the historical period and the projections in September and a simultaneous increase in rainfall projections P1 and P2 in October and November.

For ESM-CCLM, there is a simultaneous increase of the rainfall projections P1 and P2 from June to September and for P2 the increase of rains is observed until November.

For the HadGEM2-RCA, an increase of rains is observed in May and June for the projection P1 and July for the projection P2. In September and November is observed simultaneous increase of rainfall for P1 and P2.

For ESM-RCA, there is no increase in rainfall but a balance between the historical period and the P1 projections in May, June and July.

For ESM-REMO, there is no increase in rainfall for the P2 projection and instead an increase from August to October for projection P1.

The projected precipitation changes for both future time periods therefore present a complex annual pattern with some months showing increase and others indicating decrease for the same climate product.

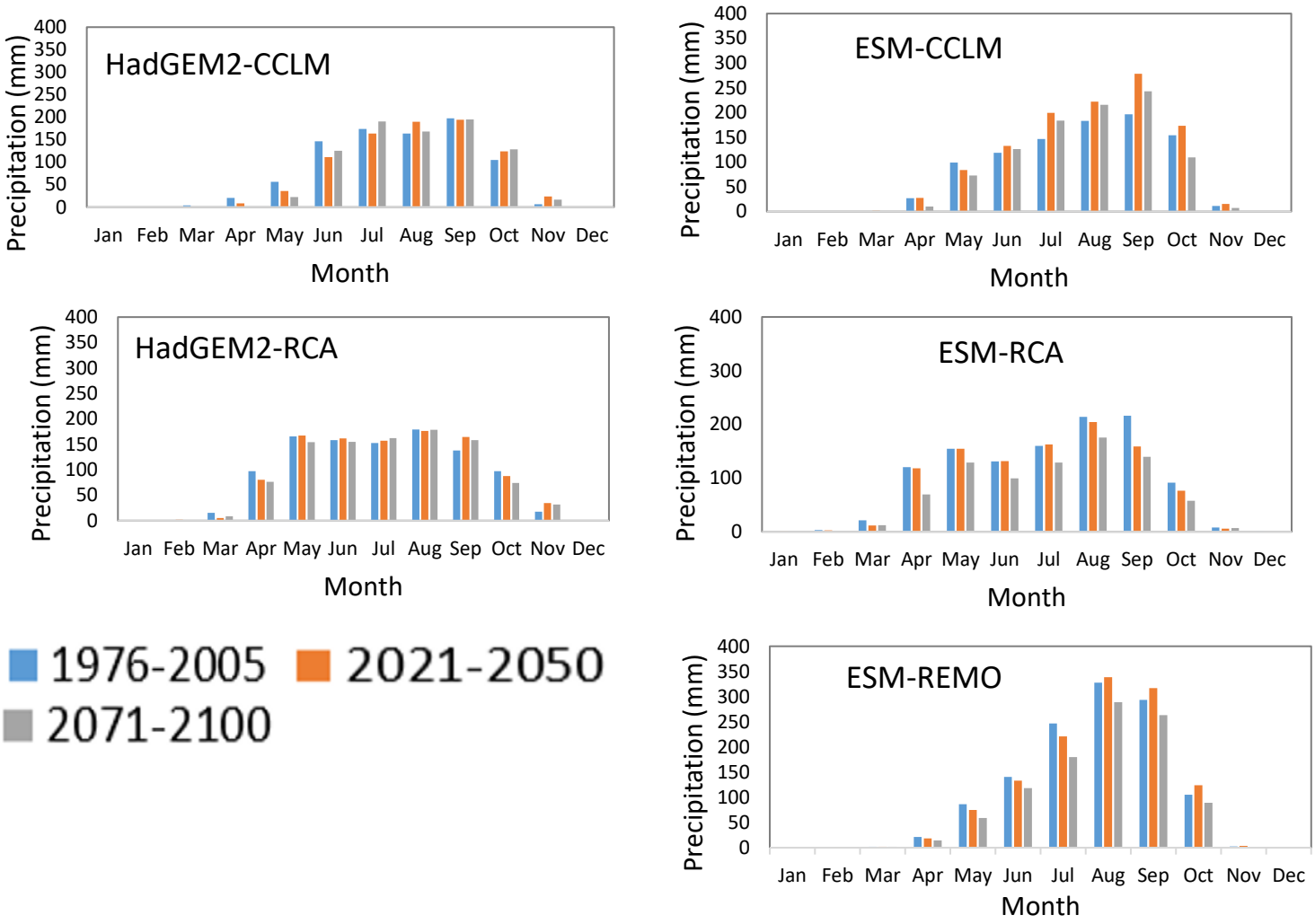

Figure 9: Diagram of the comparison between the historical (1976-2005) and projected (2021-2050 and 2071-2100) global mean annual rainfall observed and simulated between 2021-2050 and 2071-2100 of five climate models.

Figure 10 is the overall average rainfall for the historical period (1976-2005) and projected (2021-2050 and 2071-2100). With a rainfall increase of 19.98 mm (1.936%) for P1 and a significant reduction of rainfall of -105.85 mm (-10.22%) for P2.

On the whole, the HadGEM2-CCLM shows a decrease of the rainfall of -23.69 mm (-2.71%) for simulated projection P1 and of -26.80mm (-3.07%) for simulated projection P2.

For the ESM-CCLM, on the whole product there is an increase in rainfall of 196.39 mm (20.92%) for P1 and an increase of 30.76mm (3.28%) for P2.

For the HadGEM2-RCA, on the whole product there is an increase in rainfall of 14.74 mm (1.42%) for P1 and a decrease of -22.08 mm (-2.16%) for P2.

For the ESM-RCA, on the whole product a considerable reduction of the rains of -93.51 mm is observed -(8.35%) for P1 and a decrease -301.31mm (-26.89%) for P2

For the ESM-REMO, on the whole product there is a slight increase in rainfall of 6.24 mm (0.51%) for P1. A decrease in rainfall of -209.81 mm is observed (-17.12%) for P2.

The climate models ensemble mean should therefore be interpreted while care, as it hide strong divergence between climate model.

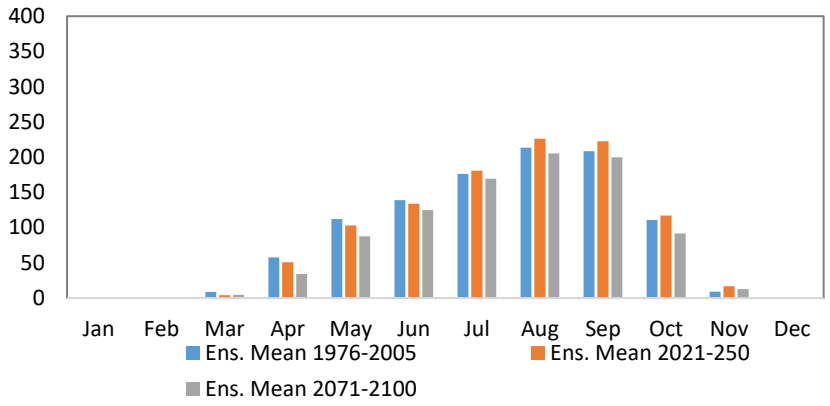

Figure 10: Comparison between the historical (1976-2005) and projected (2021-2050 and 2071-2100) global mean annual rainfall observed and simulated between 2021-2050 and 2071-2100 of climate models ensemble mean.

Figure 11 presents the historical ETp (1976-2005) and projections (2021-2050 and 2071-2100). For the set of climate products (HadGEM2-CCLM, HadGEM2-RCA, ESM-CCLM, ESM-RCA, ESM-REMO), we note that the maximum ETp is observed at the beginning of the year and then gradually decreases in general to starting in March and gradually going back up from September. The minimum value of the ETp is generally observed between August and September. This is valid for the historical period and projections. For HadGEM2-CCLM and ESM-CCLM the maximum ETp is between 200 and 250 mm and the minimum is 100 mm. For HadGEM2-RCA the maximum ETp is between 250 and 300 mm and the minimum is between 150 and 200 mm. This is valid for the historical period and projections. For ESM-RCA the maximum ETp is between 250 and 300 mm for the historical period and the projection P1 and 200 and 250 mm for the projection P2. The minimum ETp is between 150 and 100 mm for historical period and the projections P1 and P2.

ETp in general, is expected to increase excepted for ESM-REMO and ESM-RCA, this implies an increase in water stress within the catchment.

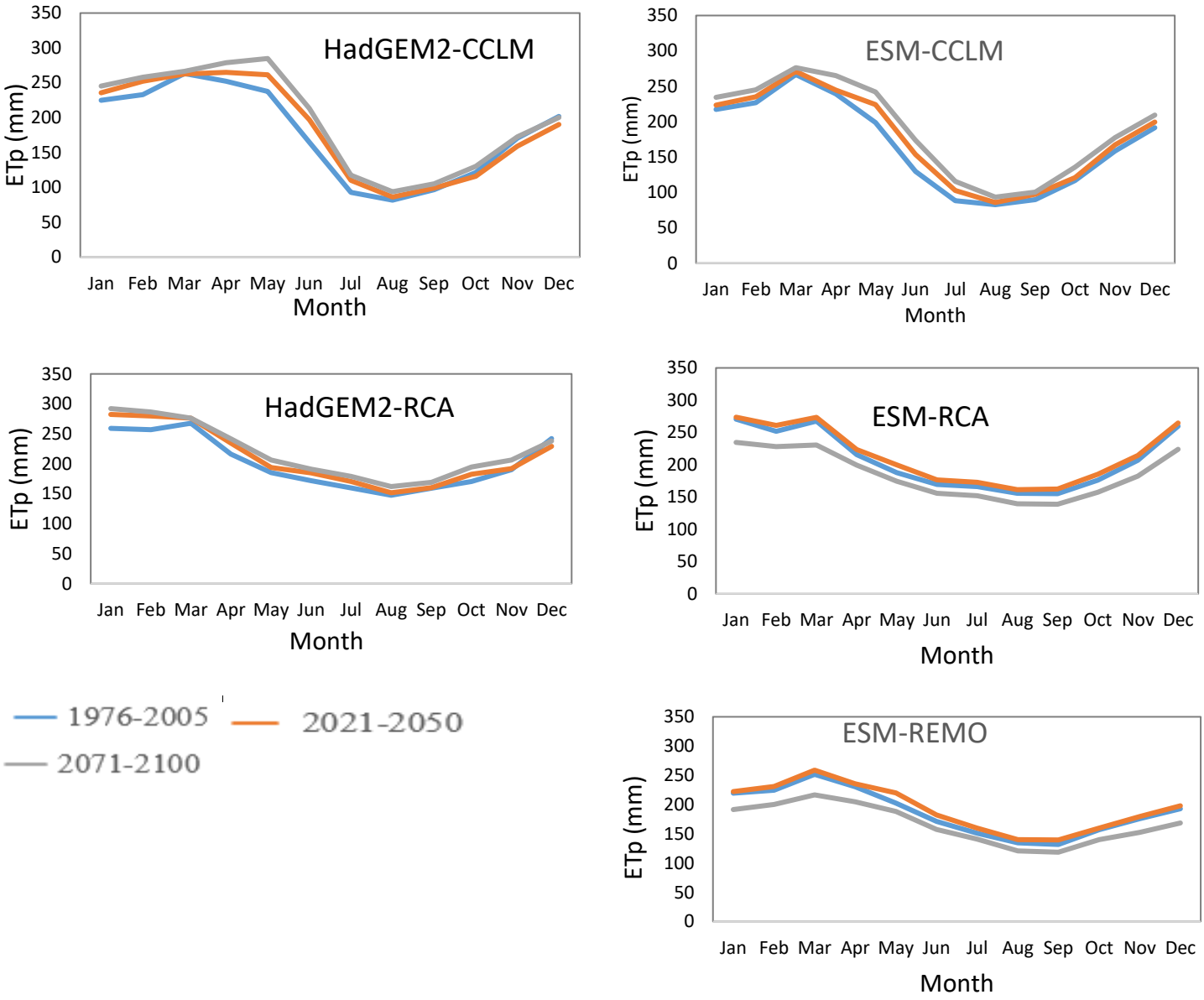

Figure 11: comparison between the overall mean annual ETp between 1976-2005 observed and those simulated between 2021-2050 and 2071-2100 of five climate models.

Figure 12 shows the diagram of ETp presenting different situation according to climate models:

For HadGEM2-CCLM, there is an increase in ETp over a large part of the year except in March, October, November and December, where there is no increase for the P1 projection. For the P2

projection the increase in ETp is observed over a large part of the year except and except in November and December when there is no increase.

For ESM-CCLM, there is an increase in ETp throughout the year for the projection P1 but in March, August and October the increase is not significant. For the P2 projection, the increase in ETp is observed throughout the year.

For HadGEM2-RCA, there is an increase in ETp over a large part of the year except in November and December. For the P2 projection the increase in ETp is observed over a large part of the year except in December when there is no increase.

For ESM-RCA, there is a slight increase in ETp throughout the year for the P1 projection. For the P2 projection, there is no increase in ETp throughout the year.

For ESM-REMO, there is a slight increase in ETp over a large part of the year for the P1 projection except in January and February where there is no increase. For the P2 projection, there is no increase in ETp throughout the year.

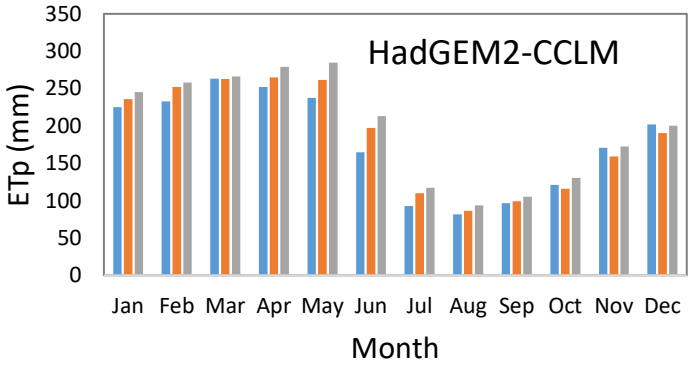

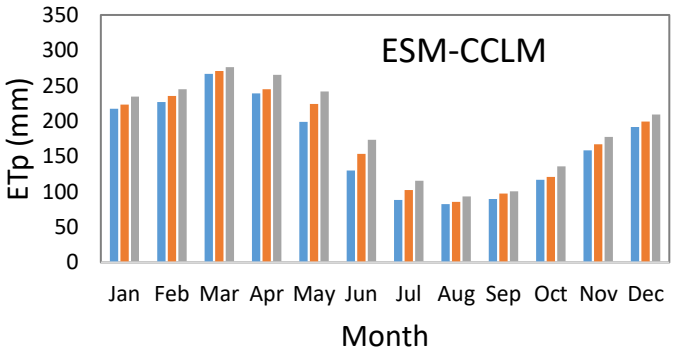

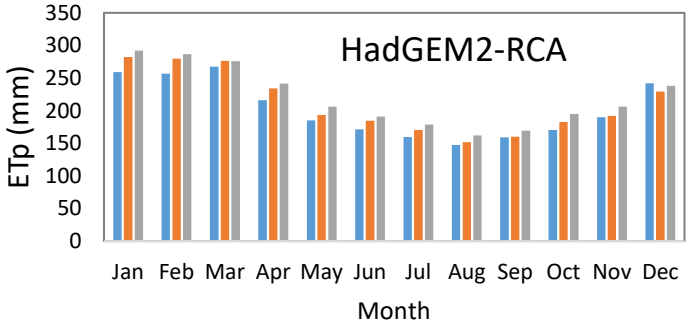

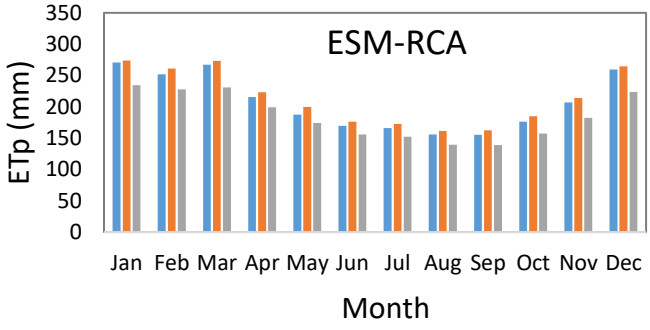

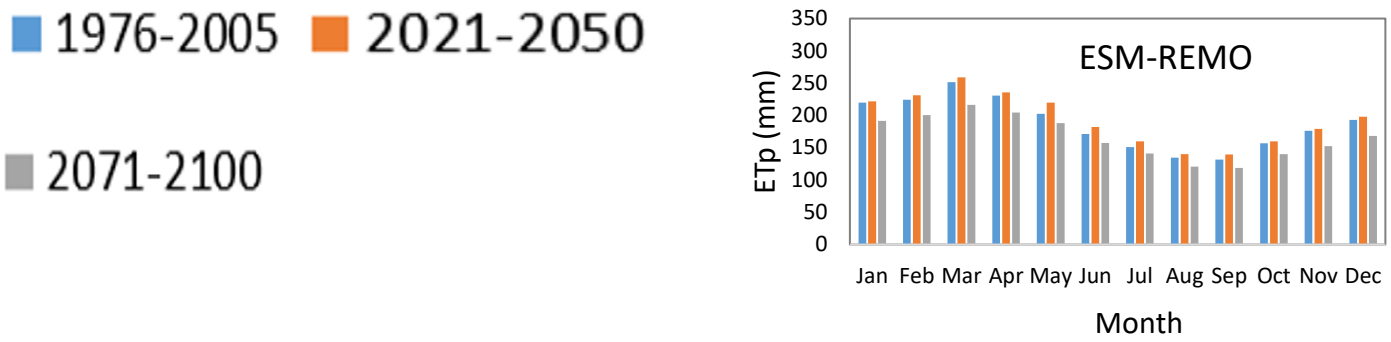

Figure 12: Diagram of the comparison between the overall annual average and 1976-2005 between 2021-2050 and 2071-2100 of five climate models.

Figure 13 represents the overall mean TEP for the historical period (1976-2005) and projected (2021-2050 and 2071-2100) for all climate models with an increase of 98.77 mm, 4.37 for P1 and an increase of 39.31 mm, 1.71% for P2.

On the whole of the HadGEM2-CCLM one observes an increase of the ETp of 94.49 mm, 4.42% for simulated projection (P1) and of 225.94mm, 10.56% for simulated projection (P2).

For the ESM-CCLM, on the whole product there is an increase in ETp of 119.13 mm, 5.94% for P1 and a considerable increase of 262.40 mm, 13.08% for P2.

For the HadGEM2-RCA, on the whole product, an increase of ETp of 111.24 mm, 4.59 % is observed for P1 and an increase of 217.91 mm, 8.99% for P2.

For the ESM-RCA, on the whole product there is an increase in ETp of 85.74 mm, 3.45% for P1 and a considerable decrease -265.74 mm, -10.71% for P2.

For the ESM-REMO, on the whole product, an increase of ETp of 83.25 mm is observed, 3.71% for P1. A considerable decrease in ETp of -243.96 mm, -10.88% is observed for P2.

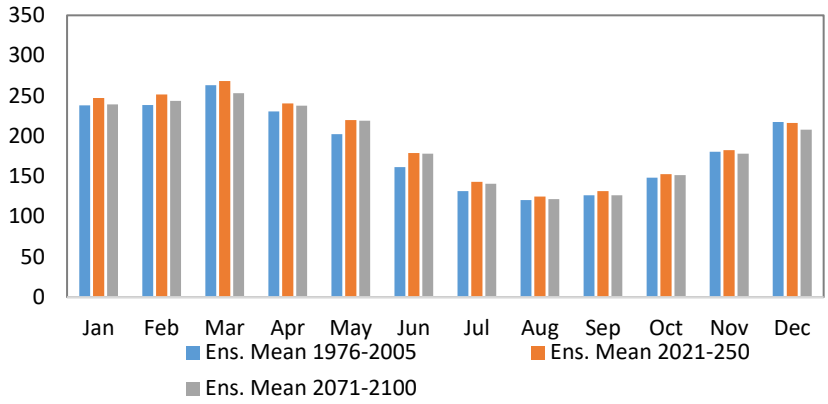

Figure 13: Comparison of the observed period (1976-2005) and the two projection periods (2021-2050 and 2071-2100) of all climate products.

Figure 14 shows historical temperatures (1976-2005) and projections (2021-2050 and 2071-2100). For the set of climate products (HadGEM2-CCLM, HadGEM2-RCA, ESM-CCLM, ESM-RCA, ESM-REMO), a good correlation is observed for the set of climatic products.

On HadGEM2-CCLM and ESM-CCLM the maximum temperatures are between 35 and 40 ° C in general and the minimum is between 20 and 25 ° C.

On HadGEM2-RCA and ESM-RCA the maximum temperatures are between 29 and 30 ° C in general and the minimum is between 20 and 25 ° C.

This is valid for the historical period and projections for climate products above.

On ESM-REMO the maximum temperature is between 30 and 35 ° C in general and the minimum is between 20 and 25 ° C.

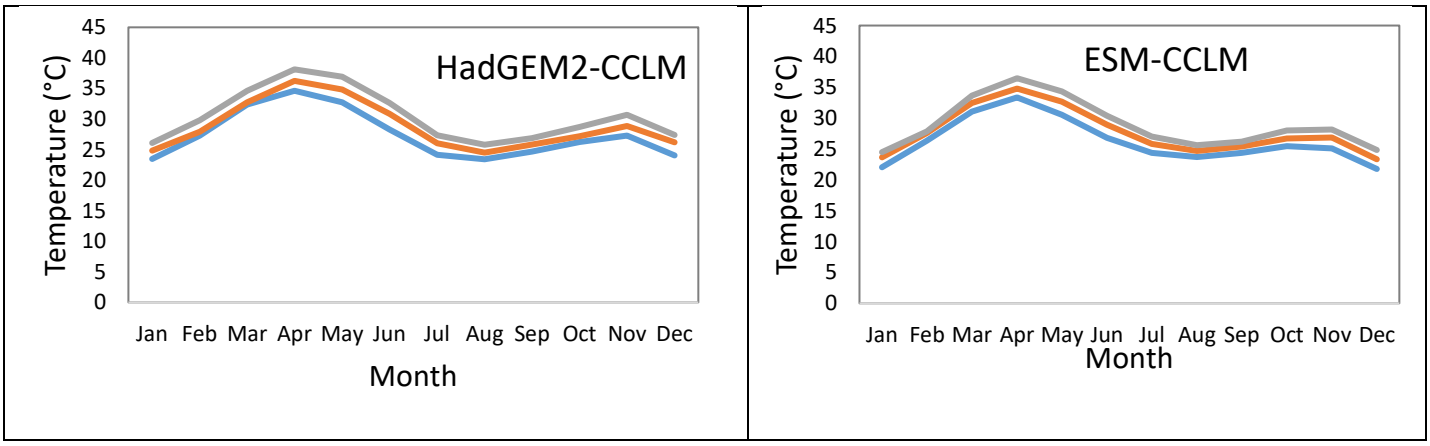

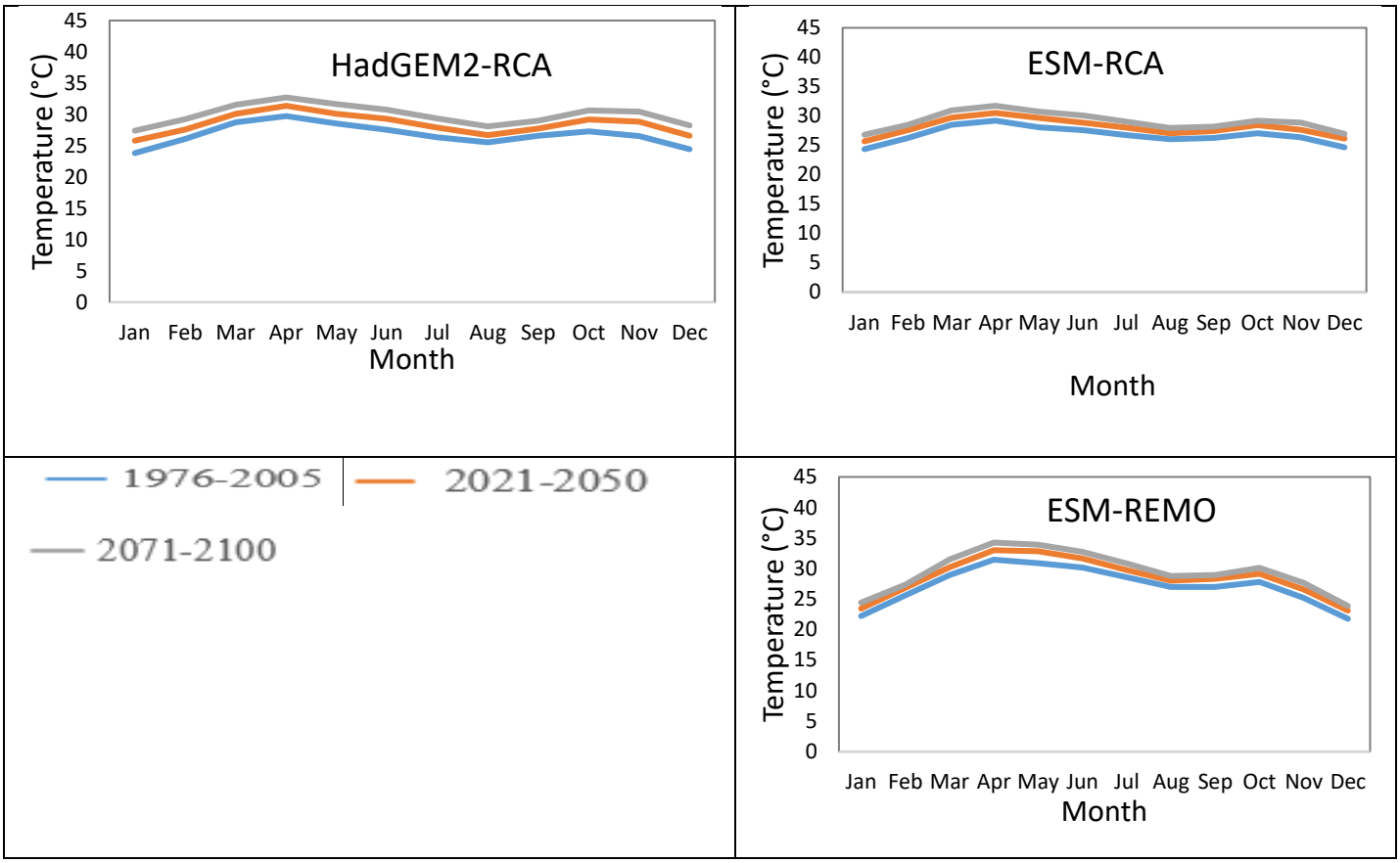

Figure 14: Comparison between historical (1976-2005) and future (2021-2050 and 2071-2100) average temperature of five climate models.

4.1.3. Climate change impact on surface water and hydrological regime

Figure 15 presents simulated discharge with the HBV-light and GR4J hydrological models for the five climate products (HadGEM2-CCLM, HadGEM2-RCA, ESM-CCLM, EMS-RCA, ESM-REMO). With the exception of the ESM-CCLM product, all products have a perfect correlation between the reference flow and the projections (P1 and P2); i.e. the same annual pattern of discharge for historical and future periods. For all climate products, runoff generally begins in May and shows a gradual decline in November for all products simulated by hydrological models. HadGEM2-RCA and ESM-RCA shows considerably higher discharges with the HBV-light hydrological model compared to GR4J.

HBV-light

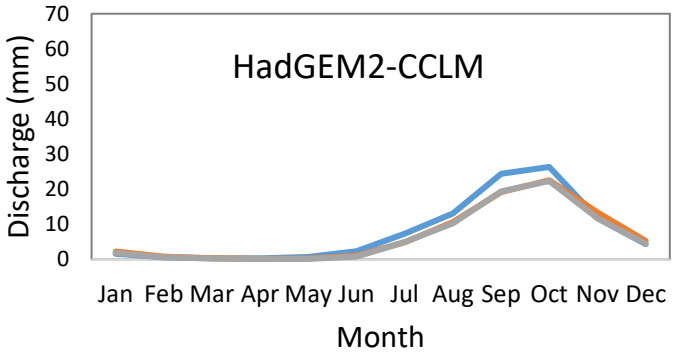

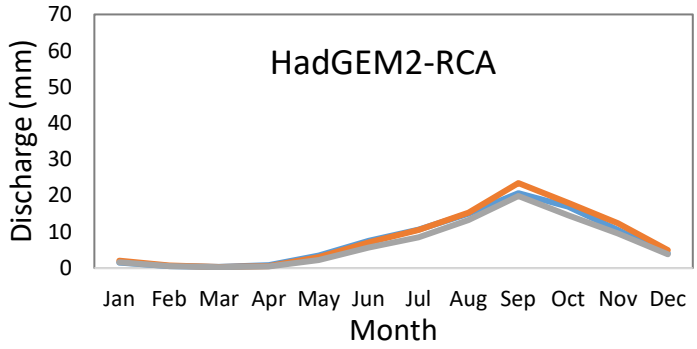

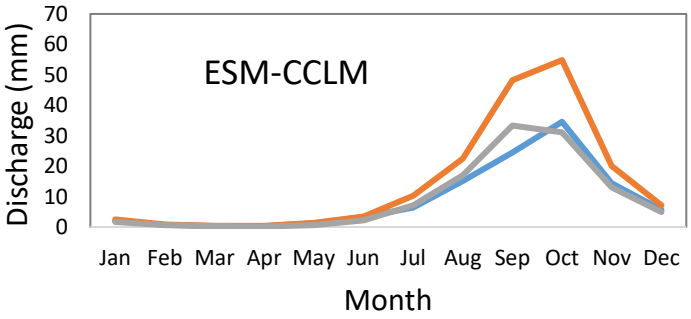

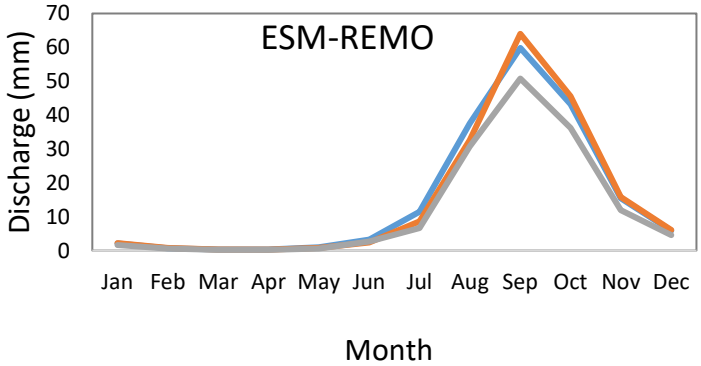

GR4J

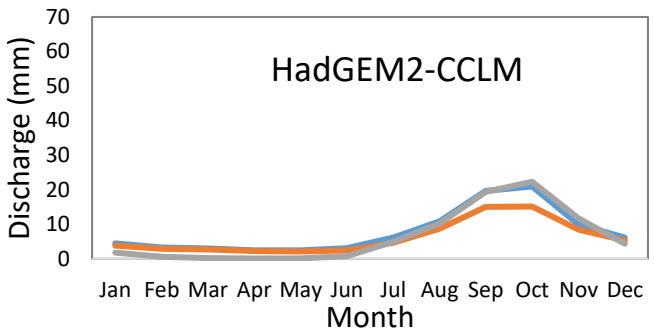

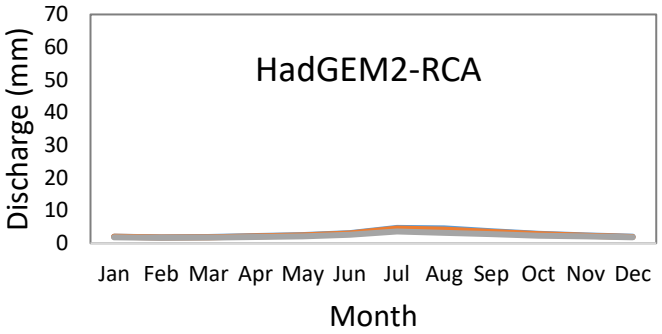

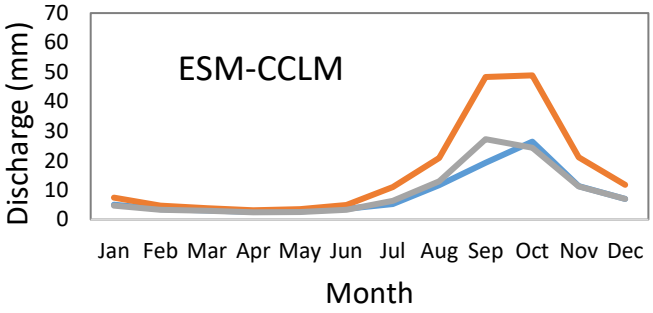

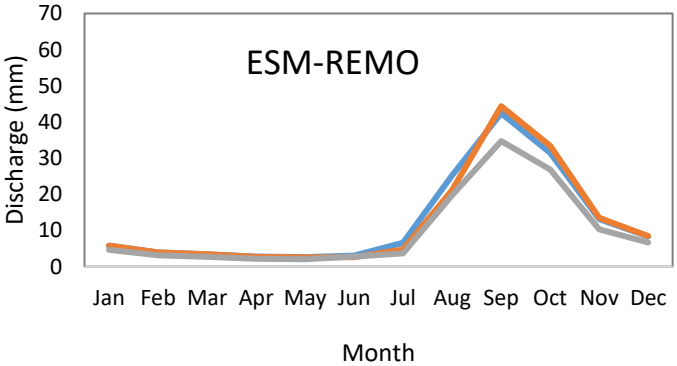

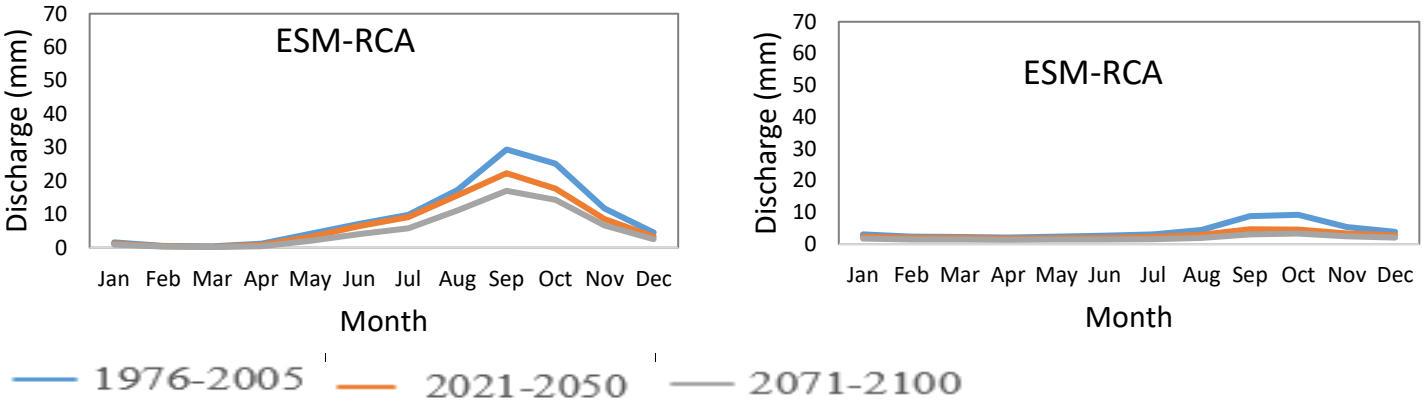

Figure 15: Comparison between the average annual discharge for historical period (1976-2005) and future periods (2021-2050 and 2071-2100) of five climate models as simulated using the hydrological models HBV and GR4J.

Figure 16 shows simulated mean flow results with the HBV-light and GR4J hydrological models for all climate products for the historical period and projections. The graph shows a strong intra-annual variability of discharge for both historical and future periods as depicted by a large min-max range. Although driven by the same climate products, it clearly appears that the simulated discharge by HBV-light is high above the one simulated by GR4J regardless the period. This is particularly the case for peak, minimum and maximum flows of the models ensemble, as follows:

The simulated maximum monthly flow with HBV-light for the historical period is between 50 and 60 mm, the ensemble mean peak flow is between 20 and 30 mm and the minimum flow is between 10 and 15 mm in September. Their counter-parts with GR4J for the same historical period are 40 and 50 mm, 10 and 20 mm, and 0 and 10 mm, respectively.

- The simulated maximum monthly flow with HBV-light for projection P1 is between 60 and 70 mm, the ensemble mean peak flow is between 30 and 40 mm and the minimum is between 10 and 20 mm in September. Their counter-parts with GR4J for the same period P1 are 40 and 50 mm, 20 and 25 mm, and 0 and 10 mm, respectively.

- The simulated maximum monthly flow with HBV-light for projection P2 is between 40 and 50 mm, the ensemble mean peak flowis between 20 and 30 mm and the minimum is between 10 and 15 mm in September. Their counter-parts with GR4J for the same period P2 are 30 and 40 mm, 10 and 20 mm and 0 and 10 mm, respectively.

These differences between discharges simulated by HBV-light and GR4J represent the uncertainty associated with the choice of the hydrological model in the current climate change impact assessment.

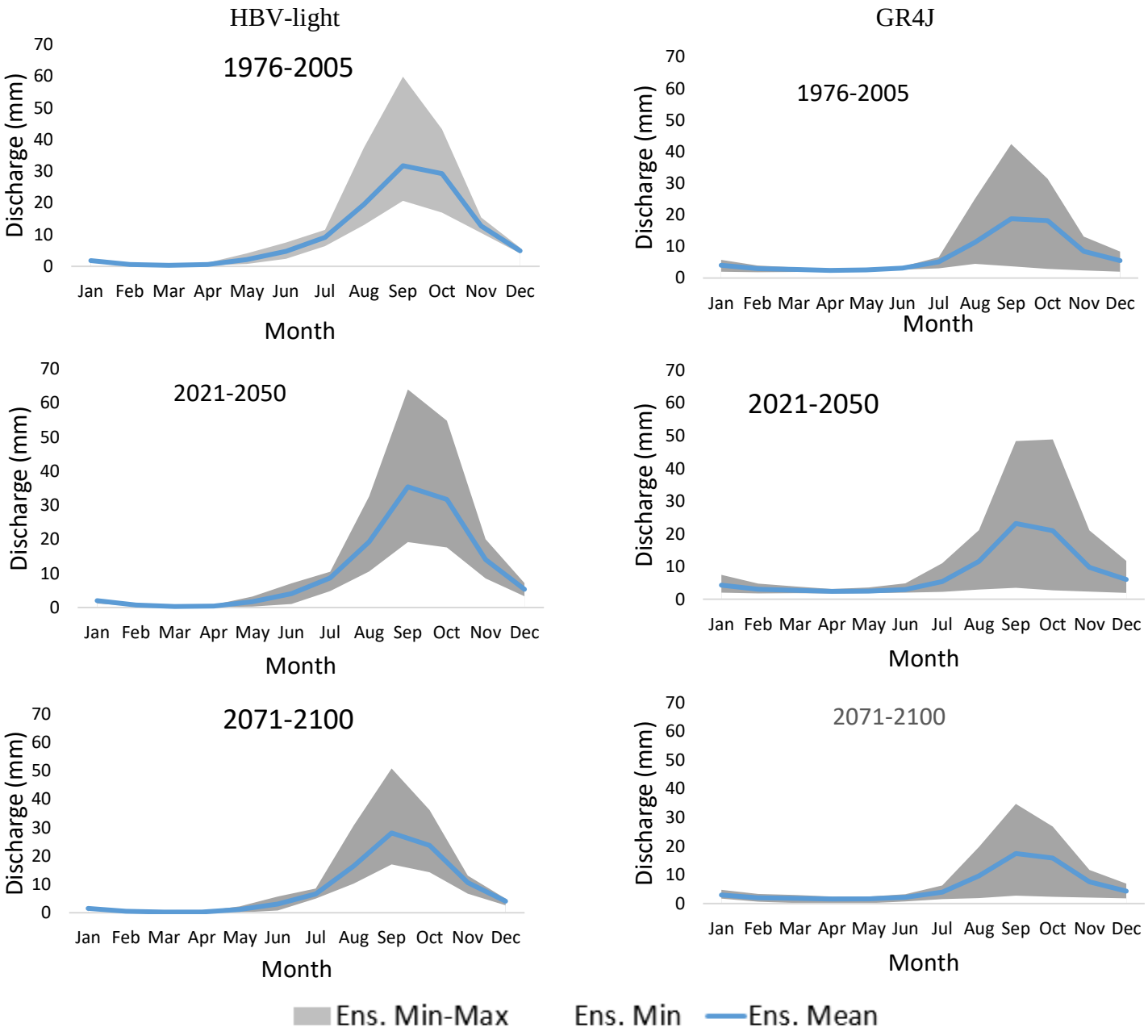

Figure 16: Comparison of the simulated discharges by the climate models ensemble (max, average, min) between the historical period and the future two periods . The simulations result from hydrological models HBV and GR4J.

Figure 17 shows the difference in flow between the historical period (1976-2005) and the two projection periods (2021-2050 and 2071-2100) of all climate models simulated with HBV and GR4J as follows:

For simulations using HadGEM2-CCLM and HBV-light there is an increase of about 0.3 mm in November and a decrease of about -0.6 mm in September on the difference of the projection P1 compared to the historical period. And an increase of about 0.1 November mm and a decrease of about -0.5 mm in September on the difference of the projection P2 compared to the historical period.

For simulations using HadGEM2-CCLM and GR4J we observe no increase and decrease of about -0.7 mm between October on the difference of the projection P1 compared to the historical period. And an observed increase of about 0.3 mm in November and a decrease of about -0.4 mm between March and April on the difference of the projection P2 compared to the historical period.

For simulations using HadGEM2-RCA and HBV-light there is an increase of about 0.35 mm in September and a decrease of about 0.1 mm between March and April on the difference of the projection P1 compared to the historical period. And an increase of about 0.1 mm January mm and a decrease of about -0.4 mm in October on the difference of the projection P2 compared to the historical period.

For simulations using HadGEM2-RCA and GR4J we observe no increase and decrease of about 0.1 mm over the whole year on the difference of the projection P1 compared to the historical period. And no observed increase and a decrease of about -0.2 mm between August and September on the difference of the projection P2 compared to the historical period.

For simulations using EMS-CCLM and HBV-light a maximum increase of about 22 mm is observed in September and no decrease on the difference of the P1 projection with respect to the historical period. And an increase of about 0.8 mm September mm and a decrease of about -0.6 mm in October on the difference of the projection P2 compared to the historical period.

For simulations using EMS-CCLM and GR4J we observe a maximum increase of about 28 mm in September and no decrease on the difference of the projection P1 compared to the historical period. And an observed increase of about 0.7 mm September and a decrease of about -0.3 mm in October on the difference of the projection P2 compared to the historical period.

For simulations using EMS-RCA and HBV-light there is no maximum increase and a decrease of about -0.7 mm in October on the difference of the P1 projection compared to the historical period. And no increase and decrease of about -12 mm in September on the difference of the P2 projection compared to the historical period.

For simulation using EMS-RCA and GR4J we observe no increase and decrease of about -0.5 mm October on the difference of the projection P1 compared to the historical period. And no observed increase and a decrease of about -0.6 mm in October on the difference of the projection P2 compared to the historical period.

For simulation using EMS-REMO and HBV-light a maximum increase of about 0.4 mm in September is observed and a decrease of about -0.5 mm in August on the difference of the projection P1 compared to the historical period. And no increase and decrease of about -0.8 mm in September on the difference of the P2 projection compared to the historical period.

For simulations using EMS-REMO and GR4J we observe an increase of about 0.4 mm between September and October a decrease of about -0.4 mm August on the difference of the projection P1 compared to the historical period. And no observed increase and a decrease of about -0.6 mm in September about the difference of the P2 projection compared to the historical period.

Differences between projected discharge change is therefore both hydrological and climate models specific (in terms of trend, magnitude and annual pattern).

HBV-ligth GR4J

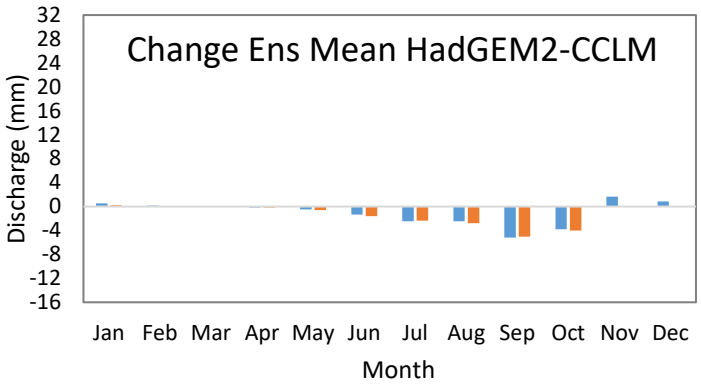
Change Ens Mean HadGEM2-CCLM
Discharge (mm)
32 28 24 20 16 12 8 4 0 -4 -8 -12 -16
Jan Feb Mar Apr May Jun Jul Aug Sep Oct Nov Dec
Month

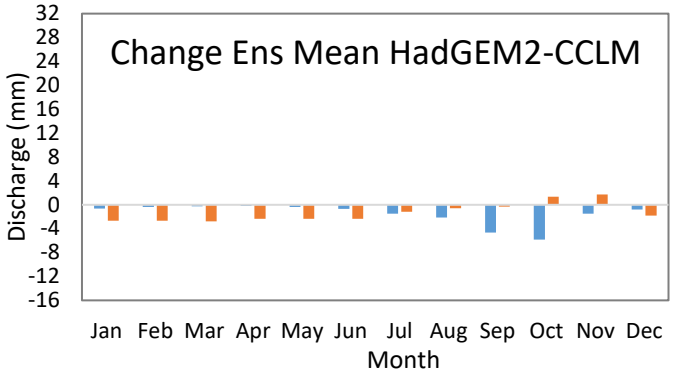
Change Ens Mean HadGEM2-CCLM
Discharge (mm)
32 28 24 20 16 12 8 4 0 -4 -8 -12 -16
Jan Feb Mar Apr May Jun Jul Aug Sep Oct Nov Dec
Month

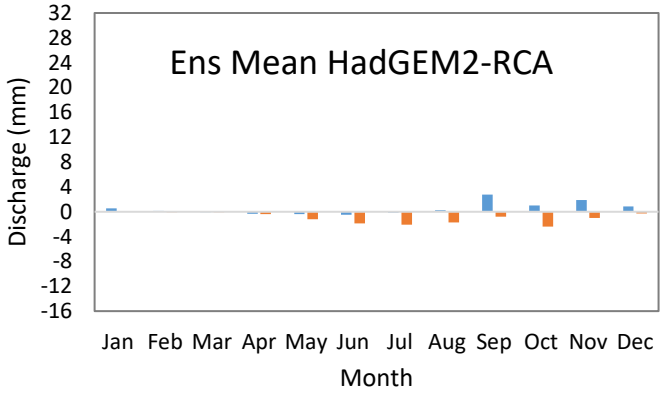
Ens Mean HadGEM2-RCA
Discharge (mm)
32 28 24 20 16 12 8 4 0 -4 -8 -12 -16
Jan Feb Mar Apr May Jun Jul Aug Sep Oct Nov Dec
Month

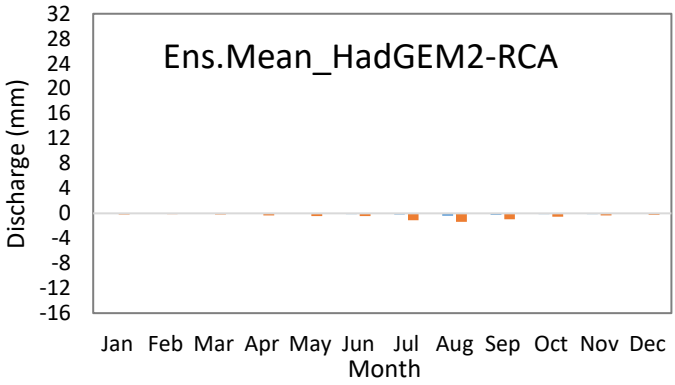
Ens.Mean_HadGEM2-RCA
Discharge (mm)
32 28 24 20 16 12 8 4 0 -4 -8 -12 -16
Jan Feb Mar Apr May Jun Jul Aug Sep Oct Nov Dec
Month

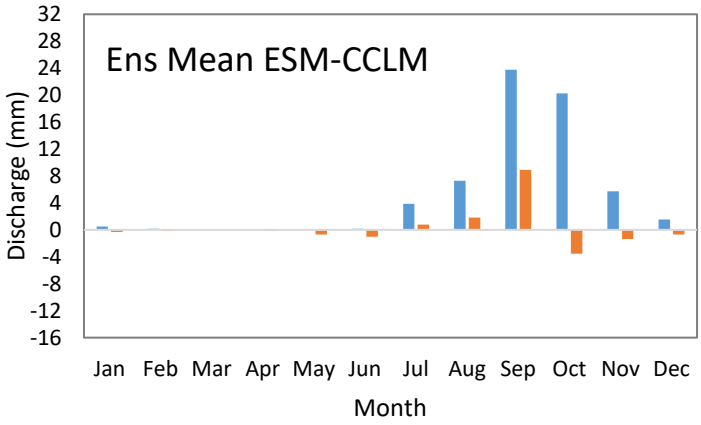
Ens Mean ESM-CCLM
Discharge (mm)
32 28 24 20 16 12 8 4 0 -4 -8 -12 -16
Jan Feb Mar Apr May Jun Jul Aug Sep Oct Nov Dec
Month

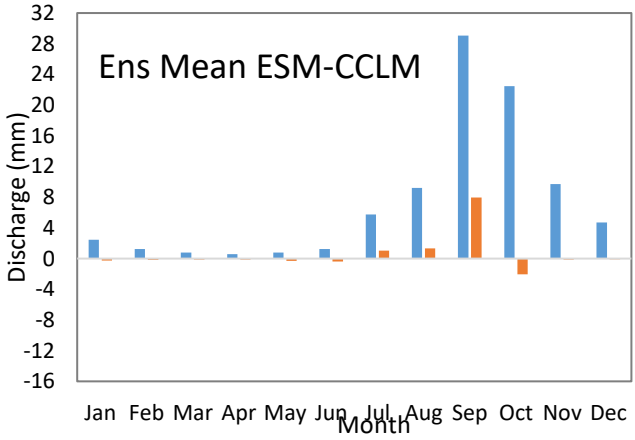
Ens Mean ESM-CCLM
Discharge (mm)
32 28 24 20 16 12 8 4 0 -4 -8 -12 -16
Jan Feb Mar Apr May Jun Jul Aug Sep Oct Nov Dec
Month

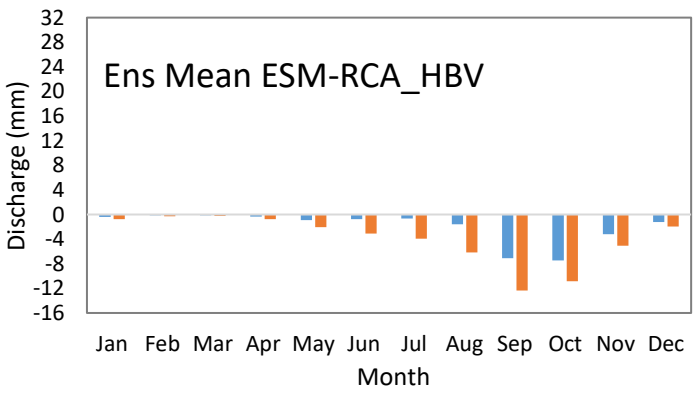
Ens Mean ESM-RCA_HBV
Discharge (mm)
32 28 24 20 16 12 8 4 0 -4 -8 -12 -16
Jan Feb Mar Apr May Jun Jul Aug Sep Oct Nov Dec
Month

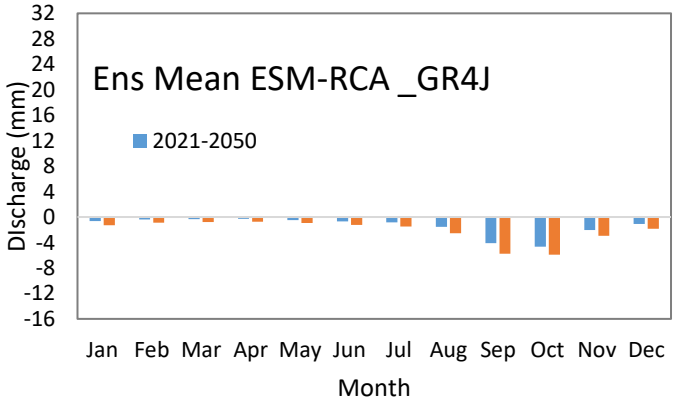
Ens Mean ESM-RCA _GR4J
2021-2050
DIscharge (mm)
32 28 24 20 16 12 8 4 0 -4 -8 -12 -16
Jan Feb Mar Apr May Jun Jul Aug Sep Oct Nov Dec
Month

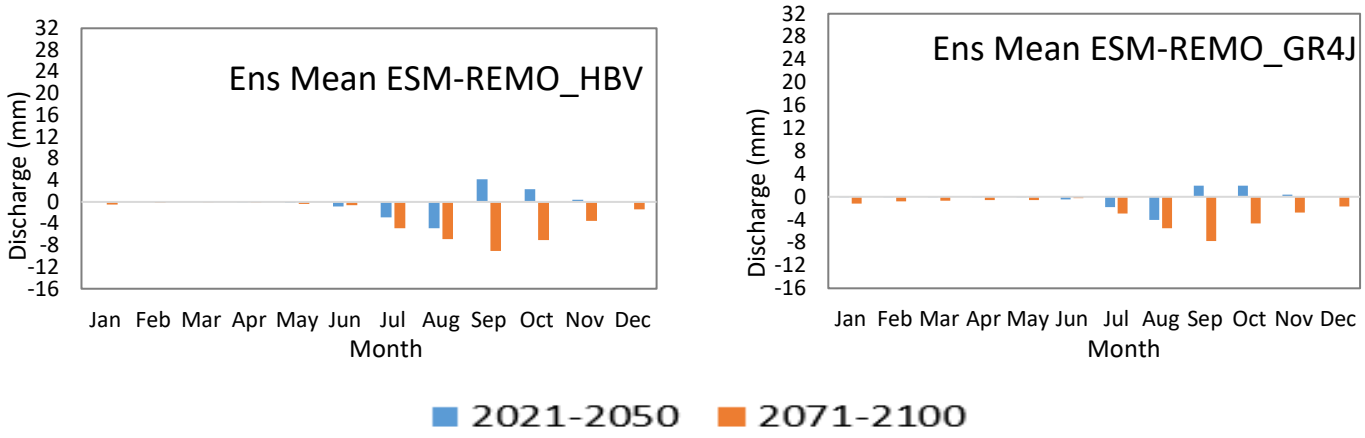

Figure 17: Comparison of the difference in discharge between the historical period (1976-2005) and the two periods of the projection (2021-2050 and 2071-2100) of all climate models simulated with HBV and GR4J.

Figure 18 shows the difference between the flows of the historical period (1976-2005) and the two future periods (2021-2050 and 2071-2100) of the average of all climate products (HadGEM2-CCLM, HadGEM2- RCA, EMS-CCLM, EMS-RCA, EMS-REMO) simulated with HBV and GR4J.

The climate products ensemble used as input for HBV-light projects a maximum increase of about 0.4 mm in September and a decrease of about -0.09 mm in July for the P1 period compared to the historical period. Whereas the same comparison for P2 shows no increase and a decrease of about -0.5 mm in October.

Using GR4J, the climate products ensemble projects a maximum increase of about 0.4 mm in September for the period P1 compared to the period historical. A decrease of about -0.25 mm from around October to November for the period P2 is projected.

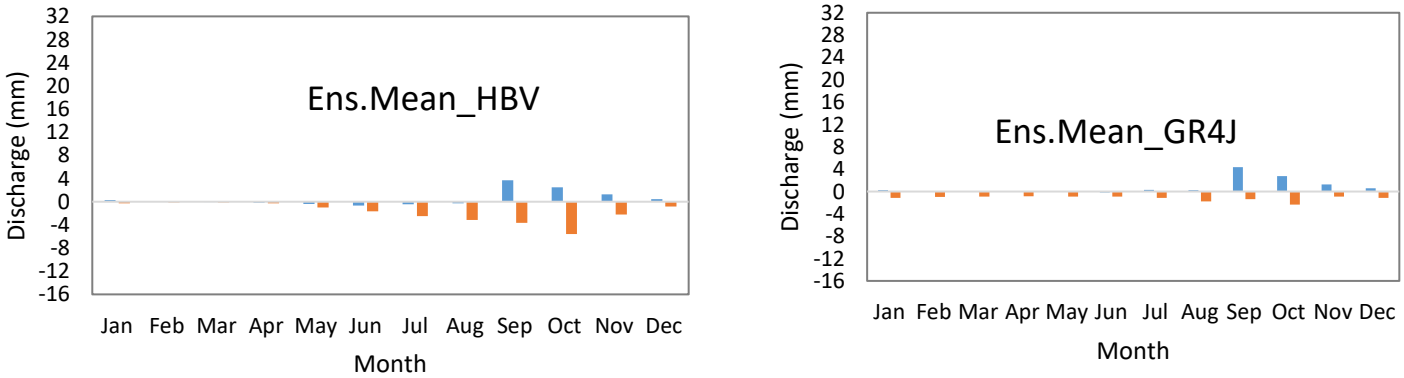

Figure 18 :Comparison of the difference between discharges the historical period (1976-2005) and the two future periods (2021-2050 and 2071-2100) of the climatic products ensemble mean as simulated with HBV and GR4J.

4.2. **DISCUSSION**

The results of the calibration of the HBV-light and GR4J hydrological models presented respectively in Fig. 5 and 7 show the performances of these two models. It was observed that the calibration of the HBV-light model had good results (NSE = 0.73 and R2 = 0.77) compared to that of the GR4J model which presented slightly lower coefficients (NSE = 0.64 and 0.73). However, the coefficients achieved with GR4J are still satisfactory in discharge modeling at a daily time step according to McCloskey et al (2011) and Moriasi et al. (2007). According to Brulebois et al. (2014) GR4J is sensitive to rainfall reproduction. However, only differences in model's structure, algorithms and calibration procedure (GAP Vs. Solver) can explain discrepancies in the models performance. As for the validation, HBV-light and GR4J yield very comparable performance NSE values equals 0.85 and 0.85 and R2 values equals = 0.88 and 0.83, respectively. The validation year (2016) was particularly wet (not shown), and this can underline the performance of the GR4J during the validation and support the hypothesis that the model is indeed sensitive rainfall representation (pattern).

The climate models as an ensemble presented a mixed precipitation change signal. Considerable decrease was note on the P2 projection compared to the historical period (1976-2005) for some models. On the other hand, there is an increase on the P1 projection compared to the historical period (1976-2005) for others. The trends can broadly be presented as follows: wet precipitation trend for ESM-CCLM, dry for ESM-RCA and mixed trends for HadGEM2-CCLM, HadGEM2-RCA and ESM-REMO. These results are consistent with those obtained by Yira et al. (2017) who worked in the same area using other climate models. They found that the overall climate models do not agree on the projected rainfall change signal as wet (RAMCO-EARTH), drier (CCLMESM and CCLM-EARTH) and mixed (CCLM-CNRM, HIRHAM-NorESM and HIRAM-EARTH) were highlighted.

With regard to temperature, we notice a temperature increase signal for all five climate models on the projections (P1 and P2) compared to the historical period. Yira et al. (2017) have reported the same results for studies conducted in the area. Also according to the study conducted by IPCC (2014), it notes that this functionality is common to all the multi-model studies conducted in the region. For the majority climate models, it is projected an increase in ETp (P1 and P2) compared to the historical period (1976-2005). Also, in Figure 12 and 15, we can see a similarity in the trend between temperature and ETp over the entire study period for all climate models. According to Yira et al. (2017), whatever the emission scenario, potential evapotranspiration only is not enough to explain the annual flow change; this is partly because the watershed's environmental system is limited in water, not energy.

The ensemble climate models and hydrological models showed a diverging discharge change signal consistently with the projected rainfall signal. Which implies that discharge in the catchment is mostly controlled by precipitation (not by temperature, which signal was clearly assessed). A clear interpretation of this results is that both increased discharge and decreased discharge have can be expected because of climate change impact on surface water resources in the catchment. The uncertainty related to the projected rainfall change signal therefore remains the major challenge to the assessment of climate change impact on water resources in the Dano catchment.

Considerable difference between discharges simulated with HBV-light and GR4J was also noticed. GR4J tends to underestimate the discharge for some climate products. This was particularly the case for HadGEM2-RCA and ESM-RCA of figure 16 which show simulated discharge almost null for the historical period and the projections (P1 and P2). The simulations with the HBV-light hydrological model, for the same product and periods showed more realistic representation of the discharge. It is worth noting that for both HadGEM2-RCA and ESM-RCA, although the simulated rainfall amount is in line with the observation, the investigations revealed that the simulated rainy days are way above observation. The distribution of rainfall is therefore the factor explaining the misrepresentation on flow regime by both climate models when applied to GR4J. This further ascertains the sensitivity of the GR4J model to rainfall representation.

CHAPTER 5 :

CONCLUSION AND RECOMMANDATION

5.1 Proposal for a recommendation on climate change adaptation strategies

While a temperature increase was confirming by the current study, there are uncertainties about rainfall projections in the Dano catchment, making it difficult to predict the trend in surface water change; and develop and implement appropriate adaptation strategies and policies (Sokona and Touré, 2009).

In the case of insufficient water for consumption, grazing and irrigation (as suggested by models predicting a decrease of water resources), it is necessary to promote the collection and use of rainwater for these needs. It is also necessary to encourage and sensitize the population to the use of soil and water conservation technics, the use of organic fertilizer etc. to increase the soil water retention capacity. Projections that indicate an increase in surface water call for action towards flood and erosion risk reduction measures; stone bunds for instance that are well adapted for the region should be promoted.

Finally, a disaster prevention and management strategy must be developed through the construction of hydraulic structures that take into account changes in hydrological regimes and also map areas at risk. Also raise awareness of the population to invest in the maintenance of these structures and avoid settling in areas at risk.

5.2 Conclusion

Due to its geographical position and its agriculture-based economy (occupies 80% of the population and about 35% of GDP), Burkina Faso is one of the most vulnerable countries to climate change in the world. The drought of the 1970s and 1980s and the sequence of recent climatic events such as rainfall variation, floods, strong winds and dust winds are warning signs of the risks weighing on Burkina Faso. An additional challenge faced by the country is climate change.

Using five climate products as input for the HBV-light and GR4J hydrological models made possible to provide answers to the initial research questions as follows:

- What are the projected climate change signals for the Dano catchment under climate change scenario RCP4.5? The results showed that there are increasing temperature and ETp trends in the catchment. While a mixed precipitation trend was found. Drier environment conditions should therefore be expected.

- What is the resulting projected change in surface water for the catchment by 2050 and 2100? Consistently with the projected precipitation change signal, both increase and decrease discharge change signals were highlighted. Despite a clear signal, rainfall remains the climate parameter controlling discharge and surface water availability.

– How is the choice of the hydrological model affecting the projected discharge change in catchment? It was pointed out that the choice of the hydrological model could affect the magnitude of the projected flow change. Although both HBV-light and GR4J were successfully validated, they yield same discharge change signal but different discharge amounts for the same climate products, implying that there are uncertainties associated with the use a single hydrological simulation model for climate change impact assessment.

– What are the strategies to minimize the impacts of climate change on water surface water resources in the catchment? In the face of these results, minimizing climate change impacts on surface water resources in the Dano catchment implies the adoption of adaptation strategies tailored for both discharge increase and decrease (like soil and water conservation technics). As ETp is likely to increase, priorities should be given to water storage technics different from open surface water bodies.

References

Albergel J., Braudeau E., 1992. Atelier de Formation aux Techniques d'Etude de l'eau dans le système Sol - Plante - Atmosphère.

Amisigo B. A., van de Giesen N. C., 2005. Using a spatio-temporal dynamic state-space model with the EM algorithm to patch gaps in daily riverflow series, with examples from the Volta Basin, West Africa.

Bates, B.C., Kundzewicz Z.W., Wu S., Palutikof J. P., 2008. Le changement climatique et l'eau. le Grouped'experts intergouvernemental sur l'évolution du climat, p. 236p.

BODIAN A., BARDIN A. D., DACOSTA H., ARDOIN S., 2013. Impact du changement climatique sur les ressources en eau du haut bassin du fleuve Sénégal 236–251.

BRULEBOIS E, AMIOTTE-SUCHET P, ROSSI A., RICHARD Y, CASTEL T, LE MOINE N, PHILIPPE M, 2014. POTENTIALITÉS D'UNE CHAÎNE HYDROCLIMATIQUE À L'ÉCHELLE DES BASSINS VERSANTS BOURGUIGNONS**.**

Callo-Concha, Daniel, Gaiser, Thomas, Ewert, Frank, 2012. Farming and cropping systems in the West African Sudanian Savanna. WASCAL research area: Northern Ghana, Southwest Burkina Faso and Northern Benin.

DIALLO A. A., SANDA I. S., 2009. ETATS DE CONNAISSANCES SUR LES CHANGEMENT CLIMATIQUES:Variabilité Climatique et Impacts sur les Ressources en Eau.

FOTSEU W., BLIN J., SANA L., SIDIBE S., 2012. CARACTERISATION ET AMÉLIORATION D'UN FOYER A CUISSON DE «DOLO» EQUIPE D'UN BRULEUR A HUILE VEGETALE (JATROPHA).

Hoekstra, A.Y., Wiedmann, T.O., 2014. Humanity's unsustainable environmental footprint. Science 344, 1114–1117. https://doi.org/10.1126/science.1248365

Hulme M., Lister D., Doherty R., Ngara T., New M., 2001. African climate change: 1900–2100.

Kasei, R., Diekkrüger, B., Leemhuis, C., 2010. Drought frequency in the Volta Basin of West Africa. Sustain. Sci. 5, 89–97. https://doi.org/10.1007/s11625-009-0101-5

Laurent F., Ruelland D., 2010. Modélisation à base physique de la variabilité hydroclimatique à l'éche d'un grand bassin versant tropical.

Moriasi D. N, Arnold J. G, Van Liew M.W., Bingner R. L., Harmel R. D., Veith T. L, 2007. Model evaluation guidelines for systematic quantification of accuracy in watershed simulations, American Society of Agricultural and Biological Engineers.

OUEDRAOGO M., 2001. Contribution à l'étude de l'impact de la variabilité climatique sur les ressources en eau en Afrique de l'ouest. Analyse des conséquences d'une sécheresse persistante: normes hydrologiques et modélisation régionale. UNIVERSITE MONTPELLIER II.

Roudier, P., Ducharne, A., Feyen, L., 2014. Climate change impacts on runoff in West Africa: a review. Hydrol. Earth Syst. Sci. 18, 2789–2801. https://doi.org/10.5194/hess-18-2789-2014

SAMBOU S., MASSECK BO., MALANG B. A., MALANDA-NIMY E. N., BODIAN A., MUSSA K., MARIKO A, BAMBA F., DACOSTA H., MALOU R., BARRY A., KANE A., MME FALL A. N., SOUMARE H., 2011. Calage et validation des modèles

hydrologiques GR4J et GR2M sur le bassin du Bafing en amont de Bafing-Makana : vers l'étude de l'impact du climat sur les ressources en eau de la retenue de Manantali.

Schmengler, A. C, 2011. Modeling Soil Erosion and Reservoir Sedimentation at Hillslope and Catchment Scale in Semi-Arid Burkina Faso.

Schmoldt, A., Benthe, H.F., Haberland, G., 1975. Digitoxin metabolism by rat liver microsomes. Biochem. Pharmacol. 24, 1639–1641.

Sivakumar, Gnoumou F., 1987. Agroclimatology of West Africa: Burkina Faso.

Somot S., 2012. Reginal Climate Modelling :motivations, techniques, illustrations, climate change scenario and uncertainties.

Sulemana Abubakari, Xiaohua Dong, Bob Su, Xiaonong Hu, Ji Liu, Yinghai Li, Tao Peng, Haibo Ma, Kai Wang, Shijin Xu, 2017. Modelling the Spatial Variation of Hydrology in Volta River Basin of West Africa Under Climate Change 16, 1095–1105.

Teutschbein, C., 2013. Hydrological Modeling for Climate change impact Assessment.

T.R. Carter, R. Leemans, M. Lal, P. Whetton, L.O. Mearns, M. Hulme, 2001. Climate Scenario Development.

Tristan d'Orgeval, 2008. Impact du changement climatique sur la saison des pluies en Afrique de l'Ouest : que nous disent les modèles de climat actuels ? 19, 79–85.

Waongo, M., Laux, P., Kunstmann, H., 2015. Adaptation to climate change: The impacts of optimized planting dates on attainable maize yields under rainfed conditions in Burkina Faso. Agric. For. Meteorol. 205, 23–39. https://doi.org/10.1016/j.agrformet.2015.02.006

Yira, Y., Diekkrüger, B., Steup, G., Bossa, A.Y., 2017. Impact of climate change on hydrological conditions in a tropical West African catchment using an ensemble of climate simulations. Hydrol. Earth Syst. Sci. 21, 2143–2161. https://doi.org/10.5194/hess-21-2143-2017

Zhu, D., Das, S., Ren, Q., 2017. Hydrological Appraisal of Climate Change Impacts on the Water Resources of the Xijiang Basin, South China. Water 9, 793. https://doi.org/10.3390/w9100793

Carbonnel, lP. et HUBERT P.; 1992. Pluviométrie en Afrique de l'Ouest soudano-sahélienne. Remise en cause de la stationnarité des séries. In L'aridité, une contrainte au développement, Ed. ORSTOM, 37-51.

Sircoulon, 1974. Les données climatiques et hydrologiques de la sécheresse en Afrique de l'ouest sahélienne. SIES rapport n02. 44 p.

Sircoulon, J. ***(1976)*** Les donnees hydropluviometriques de la secheresse recente en Afrique intertropicale. Comparaison avec les secheresses *"1913* et *1940"*. In Orstom, *ser*. Hydrol.,vol. XIII, N 2, *1976*, pp. *75-174.*

Sircoulon, -J. -*(1986)* La secheresse en Afrique de l'Ouest. Comparaison des annees *1982-84* avec les annees *1972-73.* In cah. Orstom, ser. Hydrol., vol.XXI, N *4, 1984/85*, PP. *75-86.*

PSA-DANO (2017). Plan stratégique d'assainissement des eaux usées et des excreta du centre urbain de Dano.

https://www.partagedeseaux.info/Les-consequences-du-changement-climatique-sur-les-ressources-en-eau

https://www.memoireonline.com/01/13/6693/m_Variabilite-climatique-et-gestion-des-ressources-naturelles-Cas-de-la-fort-classee-et-reserve8.html

http://leclimatchange.fr/attenuations-des-changes/

http://www.insu.cnrs.fr/environnement/climat-changement-climatique/une-nouvelle-approche-pour-les-simulations-du-climat-futu

http://www.ipcc-data.org/guidelines/pages/gcm_guide.html
https://www.meteo.unican.es/en/projects/CORDEX
http://www.csag.uct.ac.za/co

http://ar5-syr.ipcc.ch/topic_adaptation.php

www.cordex.org

www.csag.uct.ac.za/cordex/

Annexes

Cross-tabulation of the MOHC-HadGEM2-ES_CLMcom-CCLM climate model for the historial period (1976-2005)

Month	Discharge_HBV-light (mm)	Precipitation (mm)	ETp	Temperature °C	Discharge_GR4J (mm)
Jan	1.622117301	0	224.94	23.46466667	4.492157046
Feb	0.581297439	0.063333333	232.7666667	27.26650943	3.269183502
Mar	0.277009564	3.996666667	263.21	32.36512605	2.977792659
Apr	0.26805675	20.84666667	252.0366667	34.62022222	2.45238487
May	0.711657492	56.24	237.66	32.73166667	2.464035899
Jun	2.341941583	146.5933333	164.6366667	28.27044444	3.090795994
Jul	7.306984771	174.1033333	92.63666667	24.15411111	6.158895684
Aug	13.0291043	163.64	81.62	23.41222222	10.85734413
Sep	24.39441873	197.6766667	96.59333333	24.65288889	19.66750871
Oct	26.32733926	104.53	121.2166667	26.26411111	20.93800478
Nov	11.66533342	6.246666667	170.66	27.27311111	9.970343973
Dec	4.353983521	0.116666667	201.9533333	24.06522222	6.167329789

MOHC-HadGEM2-ES_CLMcom-CCLM cross-tabulated climate model for the projection (2021-2050)

Month	Discharge_HBV-light (mm)	Precipitation (mm)	ETp (mm)	Temperature °C	Discharge_GR4J (mm)
Jan	2.178451019	0	235.8266667	24.83871983	3.843650614
Feb	0.736876907	0.03	252.0933333	27.92255556	2.891009159
Mar	0.273570224	0.066666667	262.6133333	32.71055556	2.733323719
Apr	0.129394554	8.156666667	264.9266667	36.24022222	2.266115028
May	0.256870761	35.65666667	261.58	34.815	2.119299791
Jun	1.028153562	111.0133333	197.2666667	30.82222222	2.421513994
Jul	4.826296571	163.42	110.0366667	26.01633333	4.658181431
Aug	10.58050564	189.5433333	86.13666667	24.49622222	8.747197231

Sep	19.19611753	194.3733333	99.00666667	25.80233333	14.99482646
Oct	22.52907819	124.2933333	115.7466667	27.17477778	15.13480797
Nov	13.31498212	23.74333333	158.95	28.83411111	8.475164046
Dec	5.196222998	0.066666667	190.24	26.20590319	5.35246757

MOHC-HadGEM2-ES_CLMcom-CCLM Climate Model Cross-Linked Table for the Projection (2071-2100)

Month	Discharge_HBV-light (mm)	Precipitation (mm)	ETp (mm)	Temperature °C	Discharge_GR4J (mm)
Jan	1.829982818	0	245.1678571	26.09010124	1.829983
Feb	0.620369202	0.025	258.0678571	29.81630952	0.620369
Mar	0.230611036	0.153571429	266.3607143	34.62714286	0.230611
Apr	0.089598078	0.528571429	278.9392857	38.125	0.089598
May	0.102514594	22.38928571	284.7928571	36.92571429	0.102515
Jun	0.750931561	125.4678571	213.2214286	32.63404762	0.750932
Jul	4.969154882	190.5785714	117.2678571	27.33488095	4.969155
Aug	10.26537435	168.3107143	93.73571429	25.78940476	10.26537
Sep	19.38174911	194.6857143	105.2857143	26.84797619	19.38175
Oct	22.29831814	128.5678571	130.2214286	28.71380952	22.29832
Nov	11.68816802	16.47142857	172.4607143	30.6697619	11.68817
Dec	4.363703824	0.078571429	200.3464286	27.37231353	4.363704

Cross-tabulation of the MOHC-HadGEM2-ES_SMHI-RCA climate model for the historical period (1976-2005)

Month	Discharge_HBV (mm)	Precipitation (mm)	ETp (mm)	Temperature °C	Discharge_GR4J (mm)
Jan	1.527485847	0.016666667	259.233333	23.817	2.038004289
Feb	0.551434297	0.76	256.676667	26.06839623	1.809297113
Mar	0.32935432	15.22666667	267.63	28.76165966	1.893083907
Apr	0.831494889	97.36333333	216.126667	29.73066667	2.203972176

May	3.419019556	165.3633333	185.133333	28.51677778	2.492898111
Jun	7.550491639	158.2833333	171.526667	27.53633333	3.064487436
Jul	10.60937824	152.7966667	159.653333	26.352	4.694537903
Aug	14.99433378	179.1666667	147.42	25.55333333	4.543674237
Sep	20.67146095	137.72	159.09	26.56755556	3.715048079
Oct	16.97896612	97.36666667	170.306667	27.27933333	2.89014134
Nov	10.52263137	17.54	190.223333	26.56122222	2.411256639
Dec	4.093679036	0.103333333	241.886667	24.423	2.004638403

MOHC-HadGEM2-ES_SMHI-RCA cross-tabulated climate model for the projection (2021-2050)

Month	Discharge_HBV (mm)	Precipitation (mm)	ETp (mm)	Temperature °C	Discharge_GR4J (mm)
Jan	2.082358138	0.003333333	282.3333	25.80357	1.979408
Feb	0.710969772	1.603333333	279.81	27.60044	1.766908
Mar	0.296588009	5.34	276.2533	30.11056	1.84515
Apr	0.526897728	80.46	234.29	31.37178	2.114601
May	3.026099398	167.4033333	193.48	30.07789	2.413522
Jun	7.08192133	161.8766667	184.6267	29.28022	2.948128
Jul	10.483028	157.0533333	170.4233	27.907	4.500644
Aug	15.24996594	176.04	151.6167	26.67844	4.181902
Sep	23.45591933	164.6266667	159.9067	27.73956	3.485598
Oct	17.99031446	87.39	182.4133	29.19356	2.755195
Nov	12.40494345	34.28	191.9933	28.82889	2.305581
Dec	4.92838216	0.1	229.0033	26.61063	1.931783

MOHC-HadGEM2-ES_SMHI-RCA Climate Model Cross-Linked Table for the Projection (2071-2100)

Month	Discharge_HBV (mm)	Precipitation (mm)	ETp (mm)	Temperature °C	Discharge_GR4J (mm)
Jan	1.621163	0	292.0821	27.39505	1.848011
Feb	0.549871	0.235714	286.4536	29.23262	1.657765
Mar	0.244869	8.757143	276.0857	31.52429	1.700364
Apr	0.475016	76.11429	241.6571	32.7031	1.891992
May	2.231037	154.3036	206.2321	31.64369	2.071855
Jun	5.692349	154.675	191.1714	30.7575	2.605563
Jul	8.520516	162.3429	178.8893	29.35988	3.600289
Aug	13.26888	178.4107	161.9393	28.09024	3.191405
Sep	19.88878	158.4643	169.2429	28.9869	2.752422
Oct	14.57299	73.8	194.7857	30.65333	2.32778
Nov	9.508526	31.5	206.3571	30.42845	2.074875
Dec	3.837832	1.021429	237.925	28.2469	1.777432

Cross-tabulation of the MPI-M-MPI-ESM-LR_CLMcom-CCLM climate model for the historical period (1976-2005)

Month	Discharge_HBV (mm)	Precipitation (mm)	ETp (mm)	Temperature °C	Discharge _GR4J (mm)
Jan	2.020053992	0	217.343333	22.05193548	5.010354382
Feb	0.685845593	0.126666667	226.753333	26.3307783	3.488038552
Mar	0.294130315	1.126666667	266.6	31.07430108	3.086783741
Apr	0.275647888	27.02333333	239.16	33.35044444	2.575747872
May	1.277849913	99.09666667	198.876667	30.55268817	2.791458736
Jun	3.257070078	118.8933333	129.806667	26.80444444	3.657255857
Jul	6.385705961	146.7533333	88.3033333	24.34774194	5.267270533
Aug	15.15574713	183.3	82.62	23.69376344	11.65690504
Sep	24.44356803	196.35	89.6366667	24.39533333	19.28854882

Oct	34.57780205	154.39	116.77	25.45752688	26.41303186
Nov	14.36197209	11.63	158.656667	25.08122222	11.33701351
Dec	5.615965755	0	191.466667	21.76182796	7.035303104

MPI-M-MPI-ESM-LR_CLMcom-CCLM cross-tabulated climate model for the projection (2021-2050)

Month	Discharge_HBV (mm)	Precipitation (mm)	ETp (mm)	Temperature °C	Discharge _GR4J (mm)
Jan	2.532399998	0	223.46	23.6483871	7.47352605
Feb	0.858208409	0.003333333	235.2733333	27.6080283	4.74515331
Mar	0.373803325	1.623333333	270.9666667	32.4319355	3.89190342
Apr	0.369614124	27.64333333	244.77	34.7868889	3.13687732
May	1.382893998	83.95	223.9466667	32.664086	3.56676038
Jun	3.407122628	132.8966667	153.38	28.9327778	4.88948914
Jul	10.26477898	199.66	102.53	25.8352688	11.0278973
Aug	22.45790745	221.82	85.76333333	24.6808602	20.8467924
Sep	48.20970672	278.3433333	97.35	25.4322222	48.3356407
Oct	54.85017134	173.4666667	121.0533333	26.6898925	48.8820971
Nov	20.0606182	15.67333333	167.2066667	26.8373333	21.0520102
Dec	7.145306116	0	199.42	23.3333333	11.7448001

MPI-M-MPI-ESM-LR_CLMcom-CCLM Climate Model Cross-Linked Table for the Projection (2071-2100)

Month	Discharge_HBV (mm)	Precipitation (mm)	ETp (mm)	Temperature °C	Discharge _GR4J (mm
Jan	1.691868782	0	234.5133333	24.4883871	4.74416124
Feb	0.573942389	0	244.9133333	27.82030697	3.30529784
Mar	0.241662142	0.55	276.3233333	33.64537634	2.945165
Apr	0.157214908	10.25666667	265.1266667	36.46344444	2.4491481
May	0.560942855	73.15	241.7766667	34.32150538	2.48941248

Jun	2.218943265	126.0633333	173.6466667	30.37122222	3.29201879
Jul	7.158473629	184.0366667	115.62	27.00569892	6.29896095
Aug	16.99921819	215.49	93.34333333	25.62236559	12.965367
Sep	33.35006764	243.0966667	100.4733333	26.20055556	27.2454547
Oct	31.04738476	109.6733333	135.8666667	28.01591398	24.3484641
Nov	13.02426602	7.13	177.6166667	28.16211111	11.1927162
Dec	4.926765676	0	209.1766667	24.86129032	6.96362404

Cross-tabulation of the MPI-M-MPI-ESM-LR_MPI-REMO climate model for the historical period (1976-2005)

Month	Discharge_HBV (mm)	Precipitation (mm)	ETp (mm)	Temperature °C	Discharge_GR4J (mm)
Jan	2.113411258	0	219.603333	22.21935484	5.793506317
Feb	0.720769312	0.136666667	224.38	25.60082547	3.926788462
Mar	0.319053038	1.893333333	251.62	28.91075269	3.388921929
Apr	0.31353318	21.35666667	230.62	31.44511111	2.755966761
May	0.935319519	86.25	202.62	30.8872043	2.605876875
Jun	3.221056843	140.29	171	30.17933333	3.054347173
Jul	11.4753806	246.57	150.84	28.56580645	6.554985645
Aug	37.51095272	327.9133333	134.59	26.97806452	25.17779321
Sep	59.83314275	293.39	131.666667	26.994	42.41917463
Oct	43.23499077	105.4166667	156.87	27.79430108	31.4377689
Nov	15.4497292	2.45	176.01	25.18855556	13.11011577
Dec	5.8694241	0.003333333	192.803333	21.76688172	8.351471792

MPI-M-MPI-ESM-LR_MPI-REMO cross-tabulated climate model for the projection (2021-2050)

Month	Discharge_HBV (mm)	Precipitation (mm)	ETp (mm)	Temperature °C	Discharge_GR4J (mm)
Jan	2.1587656	0	222.0033	23.45172	5.7658

Feb	0.7383247	0.253333	231.0267	26.84309	3.89324
Mar	0.32463	1.756667	258.79	30.2314	3.358061
Apr	0.2660236	18.50667	235.5733	32.99689	2.705989
May	0.7415693	74.79	219.9433	32.8472	2.531729
Jun	2.3634492	133.0033	182.3067	31.64067	2.590444
Jul	8.6200188	221.0167	159.9433	29.73796	4.748539
Aug	32.637468	338.6833	140.0667	27.99602	21.11743
Sep	63.989468	316.5733	139.4667	28.30178	44.36329
Oct	45.607371	123.7767	159.5867	29.10989	33.40087
Nov	15.818425	3.546667	179.3733	26.56922	13.49142
Dec	6.0428022	0	197.7933	23.10581	8.468644

MPI-M-MPI-ESM-LR_MPI-REMO Climate Model Cross-Linked Table for the Projection (2071-2100)

Month	Discharge_HBV (mm)	Precipitation (mm)	ETp (mm)	Temperature °C	Discharge_GR4J (mm)
Jan	1.611119	0.013333	191.48	24.41045	4.595143
Feb	0.546222	0	200.2667	27.31856	3.109026
Mar	0.237257	1.883333	216.5133	31.488	2.701831
Apr	0.197447	14.33667	204.4867	34.24867	2.175695
May	0.567772	58.88	188.0333	33.87897	2.030795
Jun	2.618467	118.29	157.4433	32.72173	2.804941
Jul	6.645056	179.92	140.83	30.844	3.654191
Aug	30.6809	288.63	120.4967	28.79226	19.68896
Sep	50.78405	262.9833	118.4867	28.906	34.71226
Oct	36.18317	89.38	139.85	30.12039	26.79956
Nov	11.92743	1.546667	152.42	27.6652	10.32915
Dec	4.515773	0	168.3533	23.86826	6.681354

Cross-tabulation of the MPI-M-MPI-ESM-LR_SMHI-RCA climate model for the historical period (1976-2005)

Month	Discharge_HBV (mm)	Precipitation (mm)	ETp (mm)	Temperature °C	Discharge_GR4J (mm)
Jan	1.618396265	0	270.566667	24.34107527	3.04609199
Feb	0.565204898	3.323333333	251.86	26.22653302	2.346688816
Mar	0.39267999	21.4	267.416667	28.47612903	2.274891289
Apr	1.146750993	120.4466667	215.75	29.19211111	2.078093102
May	4.129254914	154.5766667	187.646667	28.08494624	2.35894545
Jun	7.154089044	131.2266667	169.556667	27.55966667	2.675940053
Jul	9.777697443	160.1466667	166.143333	26.74096774	3.045159364
Aug	17.24703751	213.8733333	155.853333	26.0272043	4.488353035
Sep	29.37167145	216.3033333	155.06	26.23922222	8.794868122
Oct	25.09180862	91.19666667	176.046667	27.03602151	9.234812905
Nov	11.74521356	7.916666667	206.683333	26.36222222	5.40624407
Dec	4.537688768	0.026666667	259.56	24.63344086	3.889534382

MPI-M-MPI-ESM-LR_SMHI-RCA cross-tabulated climate model for the projection (2021-2050)

Month	Discharge_HBV (mm)	Precipitation (mm)	ETp (mm)	Temperature °C	Discharge_GR4J (mm)
Jan	1.204394	0.156667	273.62	25.68452	2.398516
Feb	0.415588	2.36	261.04	27.60272	1.941719
Mar	0.256825	11.75333	273.37	29.69581	1.949337
Apr	0.814207	118.2067	223.3	30.50811	1.782567
May	3.220561	154.4633	199.9133	29.66419	1.8811
Jun	6.419123	131.79	176.2833	28.87289	2.00145
Jul	9.126186	162.6133	172.6967	28.01344	2.218656
Aug	15.65884	204.4533	161.3367	27.05817	2.952785
Sep	22.26455	158.87	162.5033	27.41356	4.675277

Oct	17.64528	76.29333	185.0633	28.42344	4.559116
Nov	8.531774	5.97	214.2233	27.64556	3.346679
Dec	3.2921	0	264.53	26.1229	2.780388

MPI-M-MPI-ESM-LR_SMHI-RCA Climate Model Cross-Linked Table for the Projection (2071-2100)

Month	Discharge_HBV (mm)	Precipitation (mm)	ETp (mm)	Temperature °C	Discharge_GR4J (mm)
Jan	0.867095	0.166667	234.57	26.79935	1.748756922
Feb	0.297548	0.406667	228.0767	28.46785	1.451818499
Mar	0.1632	12.14333	230.7333	30.95626	1.481514498
Apr	0.416485	69.69333	199.1467	31.7292	1.357674256
May	2.070769	128.7167	174.27	30.72529	1.405041225
Jun	4.056423	99.31667	155.7333	30.06267	1.42605935
Jul	5.831865	128.8167	152.0633	29.02103	1.536562581
Aug	11.10732	175.44	139.6	27.96916	1.937118711
Sep	17.00619	139.67	138.7533	28.17187	3.056354434
Oct	14.26435	57.55	157.4033	29.15781	3.337119963
Nov	6.652138	6.893333	182.1667	28.86493	2.460574364
Dec	2.568571	0.316667	223.8833	26.96194	2.063914806

Change in discharge compared to the historical period (1976-2005)

	HadGEM2-CCLM		HadGEM2-RCA		ESM-CCLM		ESM-REMO		ESM-RCA	
	2021-2050	2071-2100	2021-2050	2071-2100	2021-2050	2071-2100	2021-2050	2071-2100	2021-2050	2071-2100
Precipitation (mm)	-23.690	-26.796	14.470	-22.082	196.390	30.757	6.237	-209.807	-93.507	-301.307
Discharge_HBV-light (mm)	-12.633	-16.289	6.158	-11.668	63.561	3.599	-1.688	-34.482	-23.928	-47.476
Discharge_GR4J (mm)	-18.868	-15.915	-1.533	-6.261	87.985	6.632	-2.141	-29.294	-17.152	-26.377
Etp (mm)	94.493	225.938	111.243	217.915	119.127	262.403	83.250	-243.963	85.737	-265.743